2017-01-01

Functional and Mechanistic Insight into the Role of ATG9A in Autophagy

Vajira Kaushalya Weerasekara
Brigham Young University

Functional and Mechanistic Insight into the Role of ATG9A in Autophagy

Vajira Kaushalya Weerasekara

A dissertation submitted to the faculty of
Brigham Young University
in partial fulfillment of the requirements for the degree of

Doctor of Philosophy

Joshua L. Andersen, Chair
Barry M. Willardson
Richard K. Watt
John C. Price
Marc Hansen

Department of Chemistry and Biochemistry

Brigham Young University

ABSTRACT

Functional and Mechanistic Insight into the Role of ATG9A in Autophagy

Vajira Kaushalya Weerasekara
Department of Chemistry and Biochemistry, BYU
Doctor of Philosophy

The bulk degradative process of macroautophagy requires the dynamic growth of autophagosomes, which carry cellular contents to the lysosome for recycling. Atg9A, a multi-pass transmembrane protein, is an apical regulator of autophagosome growth, yet its regulatory mechanism remains unclear. Our data suggest that the localization of mammalian Atg9A to autophagosomes requires phosphorylation on the C terminus of Atg9A at S761, which creates a docking site for the phospho-binding protein 14-3-3ζ. Under basal conditions, the phosphorylation on Atg9A is maintained at a low level and is dependent on both ULK1 and AMPK. However, upon induction of hypoxic stress, activated AMPK bypasses the requirement for ULK1 and mediates S761 phosphorylation directly, resulting in an increase in 14-3-3ζ interaction, recruitment of Atg9A to LC3-positive autophagosomes, and enhanced autophagosome production. These observation suggested to us that long unstructured C-terminus of Atg9A may be a site of protein docking and regulation. We used BioID, along with conventional interactomics, to map the C- and N-terminal proximity-based interactions of Atg9A. We identified a network of Atg9A C-terminal interactions that include members of the ULK1 complex. Using gel filtration, we find that Atg9A co-immunoprecipitates with the ULK1 complex in high molecular weight fractions. Moreover, phosphorylation of the Atg9A C-terminus at S761 occurs within the ULK1 complex under nutrient-replete conditions, while hypoxia triggers a redistribution of phosphorylated Atg9A to low molecular weight fractions. Probing these relationships further, we find that Atg13, a component of the ULK1 complex, directly interacts with Atg9A and is required for Atg9A C-terminal phosphorylation. Furthermore, a non-phosphorylatable mutant of Atg9A (S761A) accumulates with Atg13 in high molecular weight complexes. Together, these data suggest that Atg13 recruits Atg9A to the ULK1 complex at the phagophore assemble site (PAS) and that S761 phosphorylation triggers Atg9A retrieval from the PAS

Keywords: Autophagy, ATG9A, 14-3-3ζ, AMPK, ULK1, Cancer, Chemoresistance

Acknowledgments

I would like to convey my heartfelt gratitude towards Professor Joshua L Andersen for being a wonderful and greatly insightful mentor throughout my graduate research career at his laboratory. During these four years he has been very patient and always encouraged me to be a worthy candidate to enter vast research world. His advice, constant guidance and tremendous mentorship have helped me to achieve the impossible. He has spent significant amount of his valuable time helping me writing, refining and composing research papers and my thesis dissertation. I would also like to thank my committee, Professors Barry M Willardson, Richard K Watt, Joshua L Price and Marc Hansen. They have always been resourceful, encouraging and patient even at the hardship. I would also like to thank members of Andersen laboratory. Ashari Kannangara, David Panek, David Broadbent, Nathan Rodriguez, and Siyeon Im for their invaluable support in composing the research data presented in this manuscript. I would also like thank Professor Sharon Tooze at The Francis Crick Institute, UK, Professor Tyson Sharp at Barts Cancer Institute UK, Dr. J. Will Thompson at Duke University, Medical Center, USA, Dr. Jonathan J Lee, Dr. Daniel Simmons and Dr. Catalina Matias at Department of Chemistry and Biochemistry, Dr. Jonathan Alder and Dr. David M Thomson at Life Sciences Department, Brigham Young University, USA, and Dr. Shakib Omar at National Institute of Health, USA for their collaboration, reagents, insightful knowledge and constant support throughout the project.

I would like to convey a special thanks to my dear family. Words cannot express my gratitude for my dear mother, father, and my loving wife for their constant support, understanding and care they have expressed unconditionally and constantly even at hardship. I would also like to thank my friends who always looked after me and supported me to survive and enjoy the graduate school at all times.

Table of Contents

List of Figures vi

CHAPTER 1 Introduction to Autophagy 1

1.1 References 5

CHAPTER 2 Metabolic-Stress-Induced Rearrangement of the 14-3-3ζ Interactome Promotes Autophagy via a ULK1- and AMPK-Regulated 14-3-3ζ Interaction with Phosphorylated Atg9 10

2.1 Abstract 11

2.2 Introduction 11

2.3 Results and Data 14

2.3.1 Hypoxia triggers a dynamic rearrangement of the 14-3-3ζ interactome 14

2.3.2 The interaction between 14-3-3ζ and Atg9A is increased in hypoxia 16

2.3.3 Hypoxia-induced phosphorylation of Atg9A at S761 mediates 14-3-3ζ binding. 17

2.3.4 AMPK and ULK1 are differentially required for S761 phosphorylation under basal and stressed conditions. 19

2.3.5 Phosphorylation of S761 is required for autophagy induction and Atg9A localization to LC3+ autophagosomes in hypoxia. 22

2.4 Discussion 23

2.5 Materials and Method 29

2.5.1 Cell culture and transfection. 29

2.5.2 Antibodies and chemicals 29

2.5.3 Plasmids 30

2.5.4 RNA interference. 31

2.5.5 Immunoprecipitation and immunoblotting. 31

2.5.6 *In vitro* kinase assay 31

2.5.7 Inhibitor assays. 32

2.5.8 Immunostaining and confocal microscopy. 32

2.5.9 Gel filtration assay 33

2.5.10 Mass spectrometry to identify interacting partners. 33

2.5.11 Multidimensional LC-MS/MS. 33

2.5.12 LC-MS data processing and quantitation. 34

2.5.13 Detection of hypoxia-induced phosphorylation of Atg9A by LC-MS/ MS. 35

2.6 References 36

CHAPTER 3 A BioID approach identifies a network of C- and N-terminal Atg9A interactions, including an Atg9A-Atg13-ULK1 complex that acts as a platform for Atg9A C-terminal phosphorylation. 41
3.1 ABSTRACT 41
3.2 INTRODUCTION 42
3.3 RESULTS 45
3.3.1 ATG9A may have a highly unstructured C-terminus region. 45
3.3.2 A BioID approach identifies the termini specific ATG9A interactomes 47
3.3.3 ATG9A co-fractionates with ULK1 complex proteins in size exclusion chromatography. 48
3.3.4 ATG9A co-immunoprecipitates with ULK1 complex components at high molecular weight fractions. 50
3.3.5 SDS lysis coupled BioID identifies direct versus indirect interactors of ATG9A. 52
3.3.6 Phosphorylation at S761 is necessary for the retrieval of ATG9A from ULK1 complex 53
3.4 DISCUSSION 56
3.5 Materials and method 58
3.5.1 Cell culture and transfection. 58
3.5.2 Antibodies and chemicals. 58
3.5.3 Plasmids. 59
3.5.4 RNA interference 59
3.5.5 Immunoprecipitation and immunoblotting. 60
3.5.6 Inhibitor assays. 61
3.5.7 Gel filtration assay. 62
3.5.8 Bio-ID coupled Mass spectrometry to identify interacting partners. 63
3.6 REFERENCES 64
CHAPTER 4 Discussion 67
4.1 References 71

List of Figures

FIGURE 2-1 **HYPOXIA TRIGGERS A REARRANGEMENT OF THE 14-3-3ζ INTERACTOME.** 16

FIGURE 2-2. **THE INTERACTION BETWEEN 14-3-3ζ AND ATG9A IS INCREASED IN HYPOXIA.** 17

FIGURE 2-3 **ATG9A BEARS A CONSERVED CANONICAL 14-3-3ζ BINDING PHOSPHOMOTIF.** 18

FIGURE 2-4 **HYPOXIA-INDUCED PHOSPHORYLATION OF ATG9A AT S761 MEDIATES 14-3-3ζ BINDING.** 19

FIGURE 2-5 **AMPK AND ULK1 ARE DIFFERENTIALLY REQUIRED FOR S761 PHOSPHORYLATION UNDER BASAL AND STRESSED CONDITIONS.** 21

FIGURE 2-6. **PHOSPHORYLATION OF S761 IS REQUIRED FOR AUTOPHAGY INDUCTION AND ATG9A LOCALIZATION TO LC3-POSITIVE AUTOPHAGOSOMES IN HYPOXIA.** 25

FIGURE 2-7 **MODEL OF ULK1- AND AMPK-MEDIATED REGULATION OF ATG9A VIA PHOSPHORYLATION AT S761.** 27

FIGURE 3-1 **ATG9A HAS A HIGHLY UNSTRUCTURED C-TERMINUS REGION.** 46

FIGURE 3-2 **A BIOID APPROACH IDENTIFIES THE ATG9A INTERACTOME.** 48

FIGURE 3-3 **ATG9A CO-FRACTIONATES WITH ULK1 COMPLEX PROTEINS IN SIZE EXCLUSION CHROMATOGRAPHY.** 50

FIGURE 3-4 **ATG9A CO-IMMUNOPRECIPITATES WITH ULK1 COMPLEX COMPONENTS AT HIGH MOLECULAR WEIGHT FRACTIONS.** 51

FIGURE 3-5 **SDS LYSIS COUPLED BIOID IDENTIFIES DIRECT VERSUS INDIRECT INTERACTORS OF ATG9A.** 53

FIGURE 3-6. **PHOSPHORYLATION AT S761 IS NECESSARY FOR THE RETRIEVAL OF ATG9A FROM ULK1 COMPLEX.** 55

FIGURE 4-1 **MODEL: DIFFERENTIAL REGULATION OF ATG9A PHOSPHORYLATION IN NORMOXIA OR HYPOXIA AND ITS FUNCTION IN ATG9A TRAFFICKING.**. 69

CHAPTER 1 Introduction to Autophagy

Macroautophagy (hereafter referred to as autophagy), is a cellular recycling process that is conserved from yeast to humans. It is orchestrated by a number of proteins designated with the acronym ATG. Together with the ubiquitin protease system (UPS), autophagy functions as a quality control process to maintain a healthy and functional cellular system. While the UPS requires proteins to be unfolded and ingested into the core of the 26S proteasome, in autophagy cellular contents, including organelles (e.g., mitochondria, ER) and macromolecules (e.g., ribosomes, proteins), are actively or passively encapsulated in a double membrane capsule called the autophagosome. The autophagosome then delivers its contents to the lysosome for degradation[1]. Autophagy is critical for maintaining cellular homeostasis, as defective autophagy is associated with diseases of protein aggregation[2–5].

Homeostatic quality control is not the only function of autophagy. Indeed, autophagy has mainly been described as a pro-survival response to nutrient deprivation. Once cells are subjected to starvation and amino acids become depleted, mTORC1 (mammalian target of rapamycin complex 1) becomes inhibited, which leads to the down-regulation of protein synthesis. This step is an adaptive measure that helps the cell adjust its protein synthesis to the level of available nutrients. However, under these conditions, the cell must maintain some level of metabolism. Thus, in these conditions, cells rely on autophagy as a pruning mechanism that generates the necessary metabolites (e.g., sugars and amino acids) to sustain metabolism at required levels under starvation[6–9]. Autophagy can be also activated by increased reactive oxygen species, damaged organelles such as mitochondria, ER stress, accumulation of misfolded proteins and pathogen infections[6,10–12].

The activation of autophagy is controlled by a hierarchy of signaling proteins. ULK1 (ATG1 in yeast), the only serine/threonine kinase of the core ATG proteins, is at the top and thus orchestrates the growth of autophagosomes. ULK1 forms a complex with the proteins ATG13, FIP200, ATG101, Raptor (a component of mTORC1) and AMPK (AMP-activated protein kinase) and together these proteins act as a central hub to regulate and initiate autophagy[13–15]. The presence of mTORC1 and AMPK within the ULK1 complex confers the ability to sense nutrient levels, as both kinase complexes are master sensors of cellular energy levels. When amino acid levels are high, active mTORC1 phosphorylates ULK1 at multiple sites, including S758, and inhibits ULK1 kinase activity. mTORC1 also phosphorylates other components of the ULK1 complex, such as FIP200 and ATG13, to further inhibit ULK-mediated autophagy signaling under nutrient replete conditions [14,16]

In addition, the phosphorylation of S758 helps to recruit AMPK to the ULK1 complex. Once AMPK is recruited to ULK1, it phosphorylates ULK1 at S555 and S638[15,17–19]. Although the exact function of these phosphorylations in macroautophagy is not completely clear, the phosphorylation of S555 is essential for mitophagy[20]. Thus AMPK is thought to act as a pro-autophagy counterbalance nutrient sensor to mTORC1 within the ULK1 complex and may help to maintain a low level of basal autophagy under full nutrient conditions. When nutrients become depleted, a corresponding increase in the AMP/ATP ratio fully activates AMPK and it dissociates from the ULK1 complex to phosphorylate other substrates to promote autophagy and other stress-adaptive metabolic processes[8,21]. Under these conditions, ULK1 becomes fully active and phosphorylates downstream substrates, such as Beclin1, to promote autophagosome formation[13,22,23].

Early studies showed that ULK1 and AMPK were required for the function of another ATG protein called ATG9A[24–28]. ATG9A (ATG9 in yeast) is the only multi-pass transmembrane protein of the ATG family and is thought to supply membrane in vesicle form to the growing autophagosome. ATG9A is required for full activation of autophagy as its deletion impairs autophagosome growth in cultured cells and prevents mouse embryos from surviving the neonatal starvation period, for which autophagy is critical[7,27]. Structurally, ATG9A consists of six transmembrane domains flanked by a cytosolic large C-terminal domain and a relatively smaller N-terminal domain. The N-terminal domain of ATG9A is mainly described to harbor complex N-glycans[29]. Although the functional importance of these modifications are not yet clear, we and others have noted if the entire N-terminus of ATG9A is deleted, the resulting truncation mutant will not be expressed.

Yeast ATG9 and human ATG9A bear little sequence homology, but share very similar topology (cytosolic N and C termini with 6 transmembrane domains). Furthermore, their functionality and trafficking patterns through the cell are conserved. ATG9A is highly dynamic in trafficking between membrane reservoir sites and the phagophore assemble sites (PAS)/ initiation membrane (IM) on the ER. ATG9A trafficking to the PAS/IM is referred to as anterograde trafficking and its return to membrane reservoirs is referred to as retrograde trafficking. In mammalian cells, the ATG9A reservoirs are usually either tubular vesicular structures arising from vacuolar structures and/or endosomal compartments, such as the recycling endosomes[30]. Multiple groups, including ours, have observed the importance of canonical trafficking of ATG9A between these sites to maintain a normal level of autophagy[25,28,31–33].

Most studies on ATG9A have focused on identifying the factors required for proper ATG9A trafficking. ATG9A traffics through recycling endosomal structures in a TRAPP III/TBC1D5/AP2 complex-dependent manner to PAS/IM[25]. This is also supported by other intra-cellular trafficking

machinery such as TBC1D5 and TBC1D14[34,35]. ATG9A recruitment to PAS/IM is independent of ULK1 (ATG1 in yeast), placing it with ULK1 on the top of the autophagy hierarchy[24,30,33,36]. However, ULK1 does play a regulator role in controlling the trafficking dynamics of ATG9A. In yeast, ATG9 is directly phosphorylated on its C-terminus by ATG1 and is indispensable for expansion of the autophagasome membrane[37]. In drosophila and mammals, direct phosphorylation of the myosin II motor protein by ATG1/ULK1 is required for starvation induced redistribution of ATG9A[38]. In mammals, a p38α-MAPK regulated factor called p38IP binds to ATG9A and promotes delivery of endosomal ATG9A to the PAS/IM[39]. Additional studies, primarily in the yeast system, have revealed a number of factors that are important for retrograde trafficking of ATG9A, including AMPK, ULK1, ATG13 and ATG2-ATG18 complex[14,21,30,40,41].

Although the studies mentioned above identified numerous factors required for ATG9A trafficking, there was a critical mechanistic gap in our understanding of how any of these factors control ATG9A. Toward this end, our work revealed an ULK1- and AMPK-mediated phosphorylation on Serine 761 of ATG9A. This serine is conserved from birds to humans and sits within the C-terminally cytosolic domain of ATG9A. The phosphorylation of Ser761 resulted in binding of 14-3-3ζ and subsequent localization of ATG9A onto LC3+ autophagosomal structures upon starvation and was required for autophagy induction. Using a combination of proteomics and biochemical/molecular approaches, our recent work, as described in the following chapters, indicates that the C-terminus of ATG9A may be a hub for multiple protein interactions. Most notably, our data suggest that ATG9A interacts with the ULK1 complex and that this interaction scaffolds AMPK to ATG9A, which allows for AMPK-mediated phosphorylation of Ser761. Together, our data provide a completely novel model to explain how the ULK1 complex regulates

ATG9A trafficking and thereby controls the rate-limiting step of autophagosome growth in autophagy.

1.1 References

1. Lecker, S. H., Goldberg, A. L. & Mitch, W. E. Protein Degradation by the Ubiquitin–Proteasome Pathway in Normal and Disease States. *J. Am. Soc. Nephrol.* **17,** 1807–1819 (2006).

2. Rui, Y.-N. *et al.* Huntingtin functions as a scaffold for selective macroautophagy. *Nat. Cell Biol.* **17,** 262–275 (2015).

3. Kim, P. K., Hailey, D. W., Mullen, R. T. & Lippincott-Schwartz, J. Ubiquitin signals autophagic degradation of cytosolic proteins and peroxisomes. *Proc. Natl. Acad. Sci.* **105,** 20567–20574 (2008).

4. Janji, B. *et al.* The multifaceted role of autophagy in tumor evasion from immune surveillance. *Oncotarget* (2016). doi:10.18632/oncotarget.7540

5. Tang, J.-Y. *et al.* ATG9A overexpression is associated with disease recurrence and poor survival in patients with oral squamous cell carcinoma. *Virchows Arch. Int. J. Pathol.* **463,** 737–742 (2013).

6. Kraft, C., Deplazes, A., Sohrmann, M. & Peter, M. Mature ribosomes are selectively degraded upon starvation by an autophagy pathway requiring the Ubp3p/Bre5p ubiquitin protease. *Nat. Cell Biol.* **10,** 602–610 (2008).

7. Kuma, A. *et al.* The role of autophagy during the early neonatal starvation period. *Nature* **432,** 1032–1036 (2004).

8. Shang, L. *et al.* Nutrient starvation elicits an acute autophagic response mediated by Ulk1 dephosphorylation and its subsequent dissociation from AMPK. *Proc. Natl. Acad. Sci. U. S. A.* **108,** 4788–4793 (2011).

9. Starvation-induced autophagy is regulated by mitochondrial reactive oxygen species leading to AMPK activation. Available at: http://www.sciencedirect.com/science/article/pii/S0898656812002628. (Accessed: 16th December 2016)

10. Sakai, Y., Oku, M., van der Klei, I. J. & Kiel, J. A. K. W. Pexophagy: Autophagic degradation of peroxisomes. *Biochim. Biophys. Acta BBA - Mol. Cell Res.* **1763,** 1767–1775 (2006).

11. Dunn, W. A. *et al.* Pexophagy: the selective autophagy of peroxisomes. *Autophagy* **1,** 75–83 (2005).

12. Zhang, J. *et al.* ATM functions at the peroxisome to induce pexophagy in response to ROS. *Nat. Cell Biol.* **17,** 1259–1269 (2015).

13. Ganley, I. G. *et al.* ULK1·ATG13·FIP200 Complex Mediates mTOR Signaling and Is Essential for Autophagy. *J. Biol. Chem.* **284,** 12297–12305 (2009).

14. Hosokawa, N. *et al.* Nutrient-dependent mTORC1 Association with the ULK1–Atg13–FIP200 Complex Required for Autophagy. *Mol. Biol. Cell* **20,** 1981–1991 (2009).

15. Egan, D., Kim, J., Shaw, R. J. & Guan, K.-L. The autophagy initiating kinase ULK1 is regulated via opposing phosphorylation by AMPK and mTOR. *Autophagy* **7,** 643–644 (2011).

16. mTORC1 Phosphorylates the ULK1-mAtg13-FIP200 Autophagy Regulatory Complex | Science Signaling. Available at: http://stke.sciencemag.org/content/2/84/pe51.short. (Accessed: 16th December 2016)

17. Kim, J., Kundu, M., Viollet, B. & Guan, K.-L. AMPK and mTOR regulate autophagy through direct phosphorylation of Ulk1. *Nat. Cell Biol.* **13,** 132–141 (2011).

18. Lee, J. W., Park, S., Takahashi, Y. & Wang, H.-G. The Association of AMPK with ULK1 Regulates Autophagy. *PLOS ONE* **5,** e15394 (2010).

19. Kundu, M. *et al.* Ulk1 plays a critical role in the autophagic clearance of mitochondria and ribosomes during reticulocyte maturation. *Blood* **112,** 1493–1502 (2008).

20. Egan, D. F. *et al.* Phosphorylation of ULK1 (hATG1) by AMP-Activated Protein Kinase Connects Energy Sensing to Mitophagy. *Science* **331,** 456–461 (2011).

21. Mercer, C. A., Kaliappan, A. & Dennis, P. B. A novel, human Atg13 binding protein, Atg101, interacts with ULK1 and is essential for macroautophagy. *Autophagy* **5,** 649–662 (2009).

22. Russell, R. C., Yuan, H.-X. & Guan, K.-L. Autophagy regulation by nutrient signaling. *Cell Res.* **24,** 42–57 (2014).

23. Russell, R. C. *et al.* ULK1 induces autophagy by phosphorylating Beclin-1 and activating VPS34 lipid kinase. *Nat. Cell Biol.* **15,** 741–750 (2013).

24. Chen, D. *et al.* CCCP-Induced LC3 lipidation depends on Atg9 whereas FIP200/Atg13 and Beclin 1/Atg14 are dispensable. *Biochem. Biophys. Res. Commun.* **432,** 226–230 (2013).

25. Imai, K. *et al.* Atg9A trafficking through the recycling endosomes is required for autophagosome formation. *J. Cell Sci.* **129,** 3781–3791 (2016).

26. Itakura, E., Kishi-Itakura, C., Koyama-Honda, I. & Mizushima, N. Structures containing Atg9A and the ULK1 complex independently target depolarized mitochondria at initial stages of Parkin-mediated mitophagy. *J Cell Sci* **125,** 1488–1499 (2012).

27. Kojima, T. *et al.* Role of the Atg9a gene in intrauterine growth and survival of fetal mice. *Reprod. Biol.* **15,** 131–138 (2015).

28. Staudt, C., Gilis, F., Boonen, M. & Jadot, M. Molecular determinants that mediate the sorting of human ATG9A from the endoplasmic reticulum. *Biochim. Biophys. Acta* **1863,** 2299–2310 (2016).

29. Young, A. R. J. *et al.* Starvation and ULK1-dependent cycling of mammalian Atg9 between the TGN and endosomes. *J. Cell Sci.* **119,** 3888–3900 (2006).

30. Orsi, A. *et al.* Dynamic and transient interactions of Atg9 with autophagosomes, but not membrane integration, are required for autophagy. *Mol. Biol. Cell* **23,** 1860–1873 (2012).

31. Weerasekara, V. K. *et al.* Metabolic-Stress-Induced Rearrangement of the 14-3-3ζ Interactome Promotes Autophagy via a ULK1- and AMPK-Regulated 14-3-3ζ Interaction with Phosphorylated Atg9. *Mol. Cell. Biol.* **34,** 4379–4388 (2014).

32. Staudt, C., Gilis, F., Tevel, V., Jadot, M. & Boonen, M. A conserved glycine residue in the C-terminal region of human ATG9A is required for its transport from the endoplasmic reticulum to the Golgi apparatus. *Biochem. Biophys. Res. Commun.* **479,** 404–409 (2016).

33. He, C. & Klionsky, D. J. Atg9 Trafficking in Autophagy-Related Pathways. *Autophagy* **3,** 271–274 (2007).

34. Lamb, C. A. *et al.* TBC1D14 regulates autophagy via the TRAPP complex and ATG9 traffic. *EMBO J.* **35,** 281–301 (2016).

35. Popovic, D. & Dikic, I. TBC1D5 and the AP2 complex regulate ATG9 trafficking and initiation of autophagy. *EMBO Rep.* **15,** 392–401 (2014).

36. Itakura, E., Kishi-Itakura, C., Koyama-Honda, I. & Mizushima, N. Structures containing Atg9A and the ULK1 complex independently target depolarized mitochondria at initial stages of Parkin-mediated mitophagy. *J Cell Sci* **125,** 1488–1499 (2012).

37. Papinski, D. *et al.* Early Steps in Autophagy Depend on Direct Phosphorylation of Atg9 by the Atg1 Kinase. *Mol. Cell* **53,** 471–483 (2014).

38. Tang, H.-W. *et al.* Atg1-mediated myosin II activation regulates autophagosome formation during starvation-induced autophagy. *EMBO J.* **30,** 636–651 (2011).

39. Webber, J. L. & Tooze, S. A. Coordinated regulation of autophagy by p38α MAPK through mAtg9 and p38IP. *EMBO J.* **29,** 27–40 (2010).

40. Suzuki, S. W. *et al.* Atg13 HORMA domain recruits Atg9 vesicles during autophagosome formation. *Proc. Natl. Acad. Sci. U. S. A.* **112,** 3350–3355 (2015).

41. Obara, K., Sekito, T., Niimi, K. & Ohsumi, Y. The Atg18-Atg2 Complex Is Recruited to Autophagic Membranes via Phosphatidylinositol 3-Phosphate and Exerts an Essential Function. *J. Biol. Chem.* **283,** 23972–23980 (2008).

42. Kim, J. *et al.* Differential Regulation of Distinct Vps34 Complexes by AMPK in Nutrient Stress and Autophagy. *Cell* **152,** 290–303 (2013).

43. Satoo, K. *et al.* The structure of Atg4B–LC3 complex reveals the mechanism of LC3 processing and delipidation during autophagy. *EMBO J.* **28,** 1341–1350 (2009).

44. Tsuboyama, K. *et al.* The ATG conjugation systems are important for degradation of the inner autophagosomal membrane. *Science* **354,** 1036–1041 (2016).

45. Kishi-Itakura, C., Koyama-Honda, I., Itakura, E. & Mizushima, N. Ultrastructural analysis of autophagosome organization using mammalian autophagy-deficient cells. *J Cell Sci* **127,** 4089–4102 (2014).

46. Itakura, E. & Mizushima, N. Characterization of autophagosome formation site by a hierarchical analysis of mammalian Atg proteins. *Autophagy* **6,** 764–776 (2010).

CHAPTER 2 Metabolic-Stress-Induced Rearrangement of the 14-3-3ζ Interactome Promotes Autophagy via a ULK1 and AMPK Regulated 14-3-3ζ Interaction with Phosphorylated Atg9

2.1 Abstract

14-3-3ζ promotes cell survival via dynamic interactions with a vast network of binding partners, many of which are involved in stress regulation. We show here that hypoxia (low glucose and oxygen) triggers a rearrangement of the 14-3-3ζ interactome to favor an interaction with the core autophagy regulator Atg9A. Our data suggest that the localization of mammalian Atg9A to autophagosomes requires phosphorylation on the C terminus of Atg9A at S761, which creates a 14-3-3ζ docking site. Under basal conditions, this phosphorylation is maintained at a low level and is dependent on both ULK1 and AMPK. However, upon induction of hypoxic stress, activated AMPK bypasses the requirement for ULK1 and mediates S761 phosphorylation directly, resulting in an increase in 14-3-3 ζ interactions, recruitment of Atg9A to LC3-positive autophagosomes, and enhanced autophagosome production. These data suggest a novel mechanism whereby the level of autophagy induction can be modulated by AMPK/ULK1-mediated phospho rylation of mammalian Atg9A.

2.2 Introduction

The 14-3-3 protein family includes seven human isoforms that participate in the regulation of diverse processes, including metabolism, cell cycle control, protein trafficking, cell motility, and apoptosis. 14-3-3 proteins function by binding and modulating the activity of other proteins. The biological effect of 14-3-3 binding on the target protein varies from activation, suppression, and sequestration to scaffold-like activity, any of which depends on the protein in question and the cellular context. Nearly all 14-3-3 interactions are mediated by one or two serine/threonine phosphorylations on the interacting protein. Given this dependence on phosphorylation, 14-3-3 binding is inherently dynamic. Changes in the cellular environment (i.e., nutrient availability,

adhesion, and cell-cell interactions) alter kinase signaling pathways, which in turn alter 14-3-3 interactions. This dynamic aspect of 14-3-3 biology, together with the fact that 14- 3-3 proteins regulate core biological pathways (e.g., metabolism, cell proliferation, and motility), suggests a potential role for 14- 3-3 proteins in promoting cellular adaptation to different environmental conditions.

The various biological functions of 14-3-3 proteins are largely dispersed between the different isoforms, and a growing body of data suggests that the isoform plays a central role in modulating cell survival pathways (reviewed in reference 1). 14-3-3ζ (gene symbol YWHAZ) protects cells from numerous stresses, including chemotherapy-induced death, anoikis, and growth factor de-privation (2–6). Furthermore, 14-3-3ζ expression is upregulated in many cancers, and high-level expression has been shown to correlate with poor clinical outcomes in breast cancer (4, 5, 7, 8). Moreover, overexpression of 14-3-3ζ promotes breast tumor invasiveness in both Her2-positive and -negative breast cancer set- tings (3, 5).

For these reasons, 14-3-3ζ has emerged as a potential therapeutic target in cancer (9). 14-3-3ζ, like other 14-3-3 isoforms, interacts with a large network of proteins, some of which are directly involved in survival/apoptosis signaling. These include RAF kinases, Bax, Bad, and caspase-2. Other cancer-associated pathways that depend on 14-3-3ζ for activity include mTOR, Akt, and glucose receptor trafficking.

14-3-3ζ promotes survival signaling in cells exposed to a wide range of conditions, including hypoxia (6, 10–12), in which both oxygen and glucose are limited. Because nutrient deprivation has widespread effects on kinase signaling pathways, we posited that such conditions likely alter the 14-3-3ζ interactome. Thus, using a proteomics approach, we found that treatment of cells with

1% O_2 and 2 mM glucose (here referred to as hypoxia) triggered a rearrangement in the 14-3-3ζ interactome. Many of the well-characterized 14-3-3-interacting proteins, including AS160, Bad, and PFK2, showed decreased interactions in hypoxia, while only a small subset of proteins showed hypoxia-induced interactions with 14-3-3ζ. Given the role of macroautophagy (referred to here as autophagy) in promoting cell survival in response to nutrient deprivation (13–15), we became interested in a novel hypoxia- triggered interaction between 14-3-3ζ and Atg9A, a core regulator of autophagy.

Autophagy is an adaptive catabolic process of self-digestion in which cellular components, including organelles and cytoplasmic materials, are assembled in membrane-enclosed structures called autophagosomes and carried to the lysosome for recycling. The maturation and expansion of autophagosomes are orchestrated by a complex network of proteins, many of which carry the Atg designation and are activated in response to nutrient stress. Atg9A is a multimembrane – spanning protein required for induction of autophagy, and previously reported data suggest that it drives autophagic flux by delivering membrane to growing autophagosomes (16, 17).

We found that the interaction between 14-3-3ζ and Atg9A is mediated by phosphorylation at Ser761 within a conserved 14- 3-3ζ binding site in the cytoplasmic C-terminal domain of Atg9A. Under nutrient-replete normoxic conditions, this phosphorylation is mediated by Unc51-like kinase 1 (ULK1) and AMP-activated protein kinase (AMPK), which maintain a low level of 14-3-3ζ – Atg9A interactions, but under hypoxic conditions, the full activation of AMPK results in a progressive increase in Ser761 phosphorylation and 14-3-3ζ binding. S761 phosphorylation is also triggered by other autophagy-inducing stresses, including chemotherapy treatment. Importantly, an S761A mutant of Atg9A, which is unable to bind 14-3-3ζ, is defective in autophagy and fails

to localize to LC3-positive (LC3+) autophagosomes in nutrient-deprived cells. Taken together, these data highlight the dynamic nature of 14-3-3ζ interactions and demonstrate an adaptive role for 14-3-3ζ in promoting autophagy via regulation of Atg9A in hypoxia. Moreover, these results reveal a novel mechanism linking nutrient stress and AMPK activation to the direct modulation of core autophagy machinery via phosphorylation of Atg9A. We propose that continued characterization and comparison of the 14-3-3 interaction network in response to diverse stimuli will reveal biologically important phosphorylation events and novel pathways through which 14-3-3 proteins modify the cellular response to a wide range of environmental conditions.

2.3 Results and Data

2.3.1 Hypoxia triggers a dynamic rearrangement of the 14-3-3ζ interactome

In addition to its role in promoting chemoresistance (29), 14-3-3ζ promotes cell survival under a wide range of conditions, including those that mimic tumor hypoxia. Cellular adaptation and survival under hypoxic conditions are known to generate chemoresistant and invasive tumors (reviewed in reference 30), yet the regulatory mechanisms underlying cell survival under such conditions are poorly understood. Given that glucose/oxygen deprivation induces vast alterations in kinase pathways, including the activation (e.g., protein kinase C [PKC] and AMPK) and inhibition (e.g., Akt and Erk) of kinases known to mediate 14-3-3ζ interactions, we posited that these changes would alter the 14-3-3ζ interactome, potentially revealing novel phosphorylation-triggered interactions involved in cell survival signaling.

To begin to broadly characterize how 14-3-3ζ interactions change in hypoxia, we performed gel filtration using extracts derived from HEK-293T cells treated with hypoxia (1% O2, 2 mM glucose) or left under normoxic conditions (20 mM glucose, atmospheric oxygen). In normoxia,

14-3-3ζ spanned a wide range of molecular masses, from 670 kDa to 30 kDa (the approximate size of the 14-3-3ζ monomer), consistent with its binding to numerous protein complexes (31, 32). In contrast, hypoxic conditions induced a marked shift of 14-3-3ζ toward lower-molecular-mass fractions (Fig.2-1A), indicating a potential rearrangement or loss of 14-3-3ζ interactions. To identify and characterize specific hypoxia-triggered changes in 14-3-3ζ -interacting partners, we used a coimmunoprecipitation (co-IP)-based proteomics approach. Under normoxic conditions, we identified 133 14-3-3ζ - interacting partners, many of which have been reported previously, including Bad, PFK2, AS160, IRS4, kinesin, AKAP13, and RAF kinases (reviewed in reference 33). As expected given the gel filtration results, peptide counts suggested that the vast majority of these interactions decreased in hypoxia, and quantitative analysis of a subset of 14-3-3ζ - interacting proteins confirmed the trend toward decreased interactions (Fig. 2-1B). Figure 2-1C shows Western blot validation of selected interacting proteins. Based on peptide counts, only a small subset of interacting proteins showed increased peptide counts in hypoxia, one of which was Atg9A (as confirmed by quantitative analysis in Fig. 2-1B. In addition, database search results for interacting proteins can be uploaded as a Scaffold 3 (.sf3) file via the following link: https://discovery.genome.duke.edu/express/resources/3211/3211_HDMSE_080212.sf3.

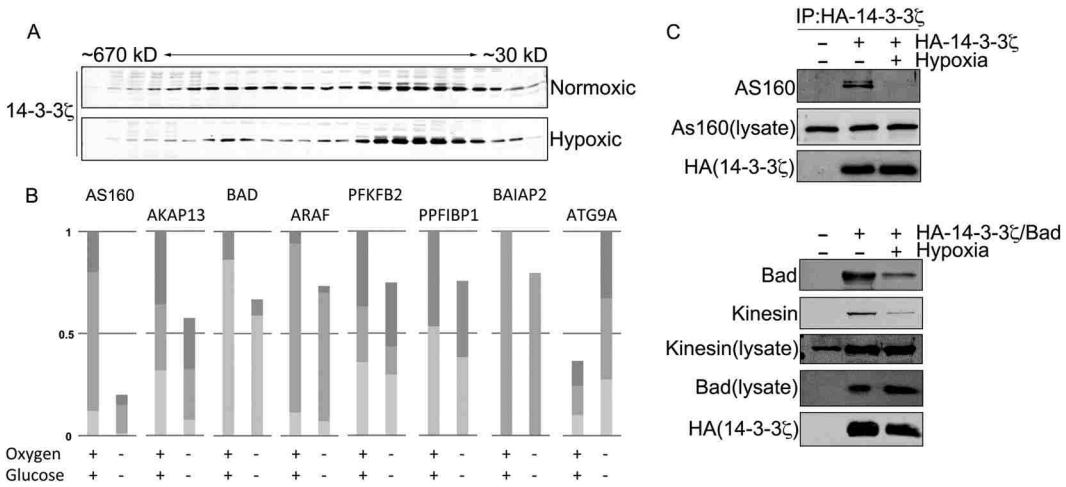

Figure 2-1 **Hypoxia triggers a rearrangement of the 14-3-3ζ interactome**. (A) HA–14-3-3ζ was overexpressed in HEK-293 cells, and cells were treated with normoxia or hypoxia for 4 h. Cell lysates were subjected to gel filtration, and the resulting fractions were immunoblotted for HA. (B) Relative quantitation of the change in 14-3-3ζ interactions for the indicated binding partners in normoxia and hypoxia. MS1 ion chromatograms for the indicated interactors were quantified by using Skyline software, as described in Materials and Methods. (C) HA–14-3-3ζ was overexpressed in HEK-293 cells and treated with normoxia or hypoxia for 6 h, followed by co-IP and immunoblotting for interacting partners. The co-IPs in the bottom panels were performed as described above except with HEK-293 cells co-transfected with Bad and HA–14-3-3ζ constructs.

2.3.2 The interaction between 14-3-3ζ and Atg9A is increased in hypoxia

Of the novel 14-3-3ζ interacting partners identified in hypoxia, our attention was drawn to Atg9A due to the role of autophagy in promoting cell survival during nutrient stress (13– 15). Furthermore, the regulation autophagy modulates tumorigenesis and promotes chemoresistance (18, 34), phenotypes that are also ascribed to 14-3-3ζ. To validate the proteomics result, tagged 14-3-3ζ or Atg9A was expressed in HEK-293 cells and then subject to co-IP and immunoblotting for their endogenous binding partner. As shown in Fig. 2-2A and B, these experiments confirmed that the interaction between 14-3-3ζ and Atg9A is increased in hypoxia.

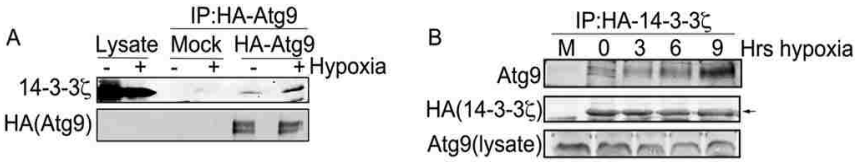

Figure 2-2. **The interaction between 14-3-3ζ and Atg9A is increased in hypoxia.** (A) HA-Atg9A was overexpressed in HEK-293 cells, and cells were treated with normoxia or hypoxia for 12 h. HA-Atg9A was immunoprecipitated and immunoblotted for endogenous 14-3-3ζ. (B) HA–14-3-3ζ was overexpressed in HEK-293 cells, and cells were treated with normoxia or hypoxia for the indicated time periods (M, mock). HA–14-3-3ζ was immunoprecipitated and immunoblotted for endogenous Atg9A

2.3.3 Hypoxia-induced phosphorylation of Atg9A at S761 mediates 14-3-3ζ binding.

Since 14-3-3ζ interactions are typically phosphorylation dependent, we examined phosphorylation of Atg9A over a time course of hypoxia treatment with an antibody that recognizes phosphoserines and phosphothreonines within 14-3-3ζ binding consensus sequences (RXXpS/TXP). Indeed, phosphorylation of Atg9A increased over time in hypoxia, correlating with a progressive increase in 14-3-3ζ binding (Fig. 2-3A). Analysis of Atg9A sequences revealed a highly conserved 14-3-3ζ binding consensus site at S761 (human Atg9A numbering) (Fig. 2-3B). Furthermore, bioinformatics analysis of 60 14-3-3 interaction motifs showed that the sequence surrounding S761 conforms to the most prominent amino acids at the critical -3, -2, and +2 amino acid positions within the 14-3-3 binding consensus sequence (Fig. 2-3C).

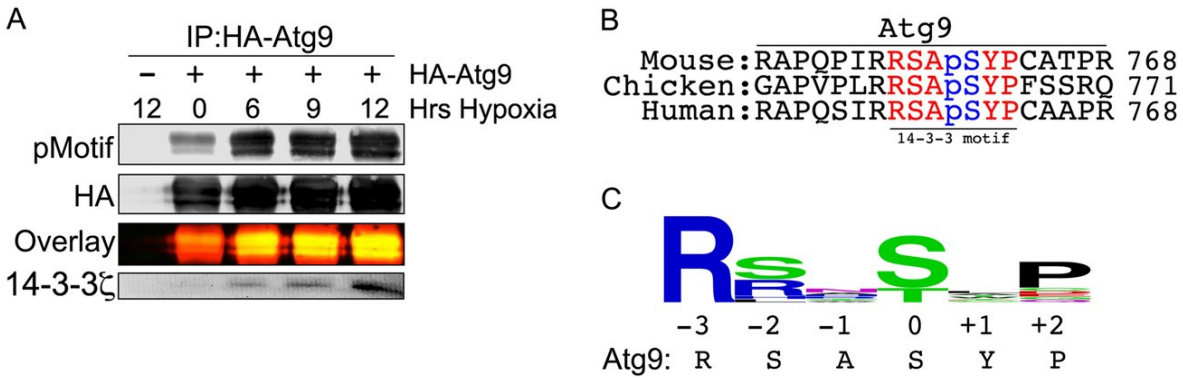

Figure 2-3 **Atg9A bears a conserved canonical 14-3-3ζ binding phosphomotif.** (A) HA-Atg9A was overexpressed in HEK-293 cells, and cells were treated with hypoxia for the indicated times. Immunoprecipitated HA-Atg9A was immunoblotted with an anti-14-3-3ζ phosphomotif antibody (pMotif) and for endogenous 14-3-3ζ. (B) Sequence alignment of Atg9A sequences from different species. Highlighted letters indicate the conserved canonical 14-3-3ζ binding motif. (C) Consensus logo for a canonical 14-3-3ζ binding motif generated by aligning 60 verified 14-3-3ζ binding motifs using WebLogo (http://weblogo.berkeley.edu/).

LC-MS/MS analysis of immunoprecipitated HA-Atg9A from hypoxic cells showed increased phosphorylation at S761 compared to that of Atg9A under normoxic conditions (Fig. 2-4A), and mutation of S761 to alanine abrogated the hypoxia-triggered interaction between Atg9A and 14-3-3ζ (Fig. 2-4B). Furthermore, the S761A mutation completely abolished Atg9A phosphorylation in HEK-293 cells and the osteosarcoma cell line U2OS (Fig. 2-4C and D). In addition, we detected an increase in the phosphosignal on endogenous Atg9A in lysates from cells treated with hypoxia (Fig. 2-4E). These data suggest that the hypoxia-triggered phosphorylation of Atg9A at S761 is necessary for 14-3-3ζ binding. Moreover, we observed increased S761 phosphorylation in response to other stresses, such as paclitaxel treatment and Earle's balanced salt solution (EBSS) starvation (Fig. 2-4F), suggesting that phosphorylation of S761 is not limited to hypoxia but rather may be a general response to autophagy-inducing conditions.

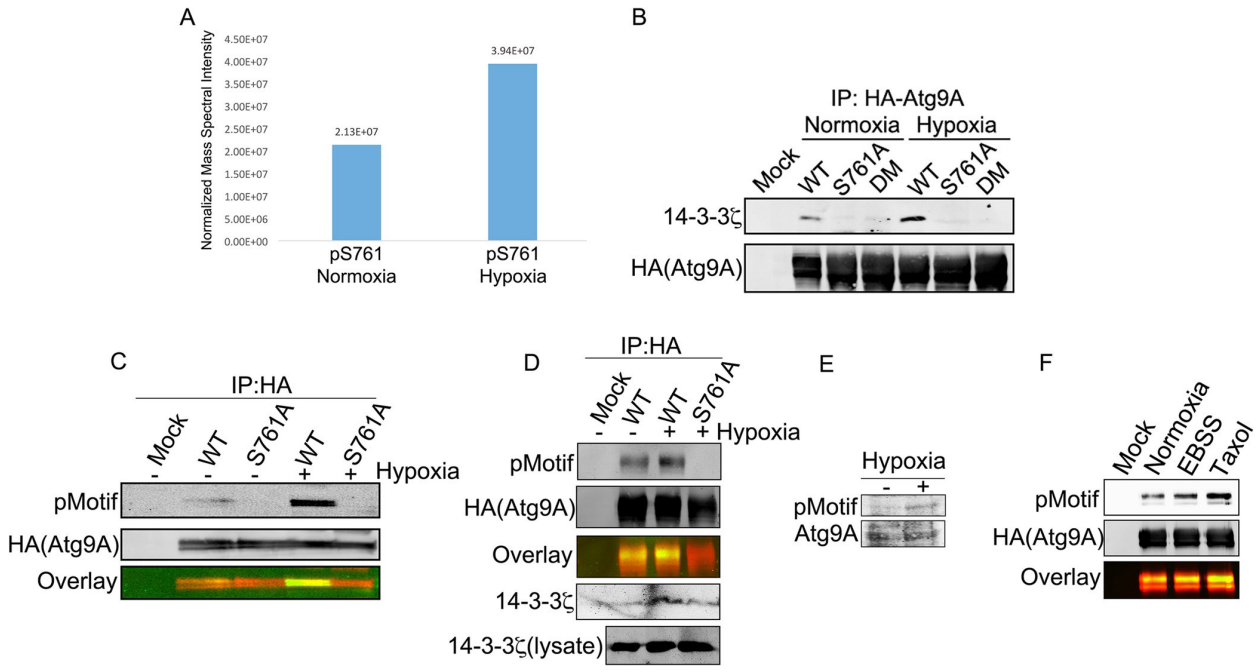

Figure 2-4 **Hypoxia-induced phosphorylation of Atg9A at S761 mediates 14-3-3ζ binding**. (A) HA-Atg9A was overexpressed in HEK-293 cells, and cells were treated with normoxia or hypoxia for 12 h. HA-Atg9A was immunoprecipitated and analyzed by LC-MS/MS. The signal intensities of the S761 phosphopeptide were measured by using software described in Materials and Methods. (B) HA-tagged WT Atg9A, an S761A mutant, and an S656A/S761A double mutant (DM) were overexpressed in HEK-293 cells, and cells were treated with normoxia or hypoxia for 12 h. Proteins were subjected to co-IP and immunoblotting for endogenous 14-3-3ζ. (C) HA-tagged WT Atg9A and the S761A mutant were treated as described above for panel B and then immunoblotted with an anti-14-3-3ζ phosphomotif antibody. (D) HA-tagged WT Atg9A and the Atg9A S761A mutant were overexpressed in U2OS cells, and cells were then treated and analyzed as described above for panel C. (E) HEK-293 cells treated with or without hypoxia for 12 h were lysed and immunoblotted with the anti-14-3-3ζ phosphomotif antibody to detect phosphorylation of endogenous Atg9A. (F) HA-tagged WT Atg9A and the S761A mutant were overexpressed in HEK-293 cells and subjected to the indicated treatments for 12 h. Immunoprecipitated proteins were immunoblotted with the anti-14-3-3ζ phosphomotif antibody.

2.3.4 AMPK and ULK1 are differentially required for S761 phosphorylation under basal and stressed conditions.

To identify the candidate kinase(s) responsible for phosphorylation of S761, we started with a panel of inhibitors against kinases activated by metabolic stresses and involved in autophagy regulation. AMPK and the class III member of the phosphatidylinositide-dependent kinase (PI3K III) family are established regulators of autophagy, and AMPK phosphorylations, in particular, are

known to mediate 14- 3-3 interactions (35, 36). Furthermore, S761 lies within a canonical AMPK phosphorylation motif (LXRXXS/T), with mouse and human Atg9A bearing a Leucine and an Isoleucine in the -5 position, respectively. As shown in Fig. 2-5A, the kinase inhibitor UCN01, at concentrations that potently inhibit AMPK (37, 38), abolished hypoxia-induced phosphorylation at S761. In addition, the AMPK inhibitor compound C also suppressed phosphorylation at S761, while LY294002, a PI3K inhibitor, had no effect (Fig. 2-5A, overlaid image showing phosphorylation in green and loading in red).

Based on these results, we suspected that AMPK could be the S761-targeted kinase. Previous studies have shown that ULK1 is upstream of Atg9A function (39, 40), and a recent report showed that yeast Atg9A is phosphorylated by ULK1 (41). Of note, however, yeast and mammalian Atg9A show very little sequence homology, and none of the known phosphorylations on yeast Atg9A align, even remotely, with S761. Nevertheless, to test the possibility that ULK1 mediates S761 phosphorylation, we measured phospho-S761 in cells treated with control or ULK1 siRNA. Strikingly, ULK1 depletion consistently resulted in a loss of the basal phospho-S761 signal in normoxic cells but failed to reduce S761 phosphorylation in hypoxic cells (Fig. 2-5B). Given that ULK2 can substitute for ULK1 in certain cell types, we also measured the phosphorylation of S761 in cells treated with ULK1 siRNA alone or ULK1 and ULK2 siRNA together (Fig. 2-5C). However, we did not observe any increased phosphorylation with combined siRNA treatment. In contrast to ULK1, expression of a dominant negative AMPK construct (AMPK-DN) abrogated both the hypoxia- induced Atg9A–14-3-3ζ interaction (Fig. 2-5D) and S761 phosphorylation under normoxic and hypoxic conditions (Fig. 2-5E). Similarly, depletion of the α1 and α2 AMPK subunits abrogated basal and hypoxia-induced phosphorylation at S761 (Fig. 2-5F). In vitro assays with purified Atg9A and recombinant AMPK and ULK1 showed that both kinases are capable of

phosphorylating S761 (Fig. 2-5G). Active liver kinase B1 (LKB1), an upstream regulator of AMPK, was used as a control and failed to phosphorylate S761 (Fig. 2-5G). Our data suggest a model in which phosphorylation of S761 is dependent on ULK1 and AMPK, potentially in complex with each other (42), under basal conditions but is coopted by activated AMPK under conditions of nutrient stress.

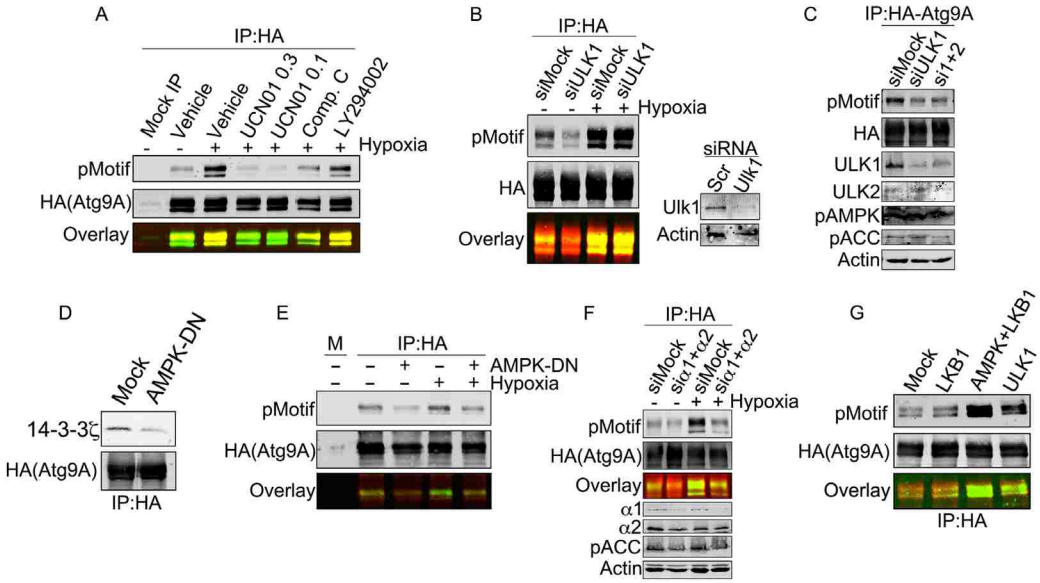

Figure 2-5 **AMPK and ULK1 are differentially required for S761 phosphorylation under basal and stressed conditions**. (A) HA-Atg9A was overexpressed in HEK-293 cells and treated with hypoxia for 12 h with the indicated inhibitors (UCN01 [0.3 μM], UCN01 [1 μM], compound C [20 μM], and LY294002 [50 μM]). Immunoprecipitated Atg9A from each treatment was immunoblotted with the phosphorylated 14-3-3 motif (pMotif) antibody. (B) HEK-293 cells expressing HA-Atg9A and transfected with the indicated siRNAs were treated with normoxia or hypoxia for 12 h. HA-Atg9A was immunoprecipitated and immunoblotted for phosphorylated S761. (C) HEK-293 cells expressing HA-Atg9A and transfected with the indicated siRNAs were treated with normoxia. HA-Atg9A was immunoprecipitated and immunoblotted for phosphorylated S761 and the indicated controls. (D) HEK-293 cells expressing HA-Atg9A with or without the AMPK alpha2 K45R mutant (a dominant negative AMPK construct) were treated with hypoxia for 12 h. Immunoprecipitated HA-Atg9A was immunoblotted for endogenous 14-3-3ζ. (E) Cells treated as described above for panel C were subjected to co-IP with HA-agarose resin followed by immunoblotting for phosphorylated S761. (F) HEK-293 cells expressing HA-Atg9A and transfected with siRNAs against the α1 and α2 subunits of AMPK were treated with normoxia or hypoxia for 12 h. HA-Atg9A was immunoprecipitated and immunoblotted for phosphorylated S761. Phosphorylated acetyl-CoA carboxylase (pACC), an AMPK substrate, and AMPK subunits were assessed by Western blotting in lysates to validate AMPK depletion. (G) Resin-bound HA-Atg9A purified from HEK-293 cells was treated with Calf alkaline phosphatase for 10 min, thoroughly washed, and then incubated with the indicated recombinant enzymes for 30 min. After further washing, resin-bound HA-Atg9A was resolved by SDS-PAGE and immunoblotted with phospho-S761 antibody.

2.3.5 Phosphorylation of S761 is required for autophagy induction and Atg9A localization to LC3+ autophagosomes in hypoxia.

To begin to assess the biological relevance of S761 phosphorylation and 14-3-3ζ binding to Atg9A, we measured LC3 lipidation (LC3-II) levels as a marker of autophagy in cells expressing wild-type (WT) Atg9A or the 14-3-3ζ-binding-defective Atg9A S761A mutant with or without bafilomycin A1, an inhibitor of autophagosome-lysosome fusion. While WT Atg9A expression resulted in an increase in the LC3-II/LC3-I ratio in hypoxia, expression of the S761A mutant inhibited conversion of LC3-I to LC3-II. These data led us to compare WT Atg9A and S761A mutant functions more specifically by assessing their subcellular distribution. Atg9A normally associates with the trans-Golgi network (TGN) and early endosomes (EE) and then redistributes to LC3- positive autophagosomal structures and the cell periphery upon induction of autophagy to promote the growth of autophagosomes (16, 40, 43). Consistent with previously reported data (40, 44), hypoxia induced a shift in WT Atg9A from a partially perinuclear/diffuse pattern to a more punctate localization in U2OS cells. However, the Atg9A S761A mutant remained predominately perinuclear/diffuse regardless of the treatment (Fig. 2-6B), suggesting a fundamental defect in the function of the phosphomutant. In- deed, we failed to observe any notable Atg9A S761A punctate structures in the hypoxia-treated cells (Fig. 2-6B).

To more accurately assess whether the failure of the S761A mutant to form punctate structures reflect an overall defect in its autophagic activity, we analyzed Atg9A localization in HeLa cells stably transfected with GFP-LC3 (18). Under normal conditions, LC3 is diffusely expressed in the cytoplasm and becomes punctate only as it incorporates into autophagosomal structures during autophagy. Thus, GFP- LC3 puncta are a marker for mature autophagosomes (45). Consistent with our data from U2OS cells, the S761A mutant and WT Atg9A showed a striking difference in

localization, with the S761A mutant adopting a more perinuclear/diffuse pattern in hypoxia. Furthermore, while hypoxia treatment produced an increase in the number LC3-positive autophagosomes in WT Atg9A-expressing cells, the autophagosome numbers were reduced to background levels in hypoxic cells expressing the S761A mutant (Fig. 2-6D). A more precise and specific measure of Atg9A function is its ability to redistribute to autophagosomes during autophagy. Importantly, the percentage of LC3-positive autophagosomes that colocalized with WT Atg9A increased by nearly 3-fold in hypoxia (Fig. 2-6E), which is consistent with data from previous studies (40, 43). In contrast, the S761A mutant showed a lack of response to hypoxia, with the percentage of LC3 and Atg9A S761A mutant-copositive structures hovering below the baseline levels for WT Atg9A in normoxia (Fig. 2-6E). Together, these data suggest that phosphorylation of Atg9A at S761 is required for the association of Atg9A with autophagosomal structures and that, in the absence of phosphorylation and 14-3-3ζ binding, Atg9A fails to properly mobilize in response to autophagic signals.

2.4 Discussion

In this study, we set out to identify stress-induced 14-3-3ζ-interacting proteins. Given the dynamic and generally prosurvival nature of 14-3-3ζ binding, we reasoned that this approach would select for biologically important phosphorylation events that help cells adapt to and survive under stress conditions. The data presented here reveal a previously uncharacterized mode of autophagy regulation that links ULK1 and AMPK directly to the core autophagy protein Atg9A. Our data suggest that Atg9A localization to autophagosomes requires phosphorylation on the C-terminal portion of Atg9A at S761, which creates a 14-3-3ζ docking site. Under basal conditions, this phosphorylation is maintained at a low level by ULK1 and AMPK. However, upon induction of hypoxic stress (low glucose and oxygen), activated AMPK by- passes the requirement for ULK1

and mediates S761 phosphorylation, resulting in increased 14-3-3ζ interactions and recruitment of Atg9A to LC3-positive autophagosomes (see the model in Fig. 2-7). To our knowledge, this is the first reported regulatory mechanism that involves phosphorylation of mammalian Atg9A. Moreover, this study expands our understanding of the role of AMPK in the regulation of core autophagic machinery.

In recent years, our understanding of the role of AMPK in autophagy has rapidly expanded. AMPK was initially linked to autophagy indirectly through inhibition of the mTOR complex (36, 46), and early work on autophagy placed the yeast ortholog of AMPK, Snf1, upstream of Atg1 (the ortholog of ULK1) (47). Recent reports have expanded the picture by showing that AMPK associates with and phosphorylates ULK1 (35, 39, 48, 49). However, the precise nature of the AMPK-ULK1 link is not completely clear, with conflicting reports about whether AMPK-mediated phosphorylation of ULK1 stimulates or suppresses autophagy.

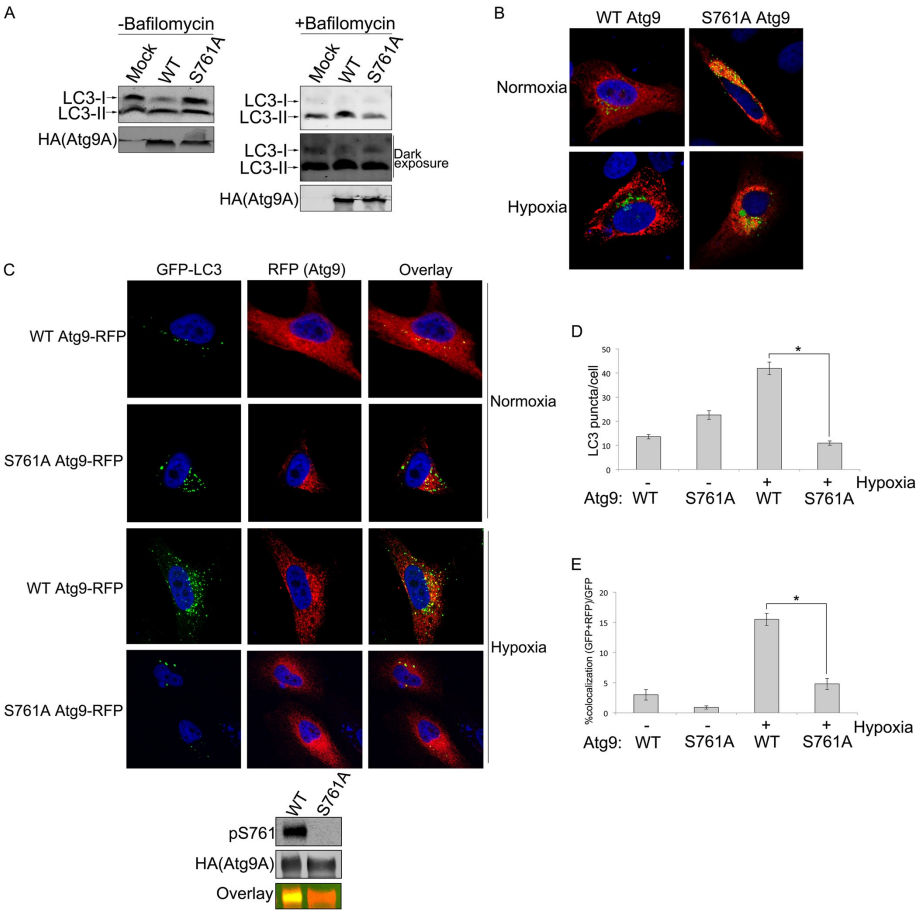

Figure 2-6. **Phosphorylation of S761 is required for autophagy induction and Atg9A localization to LC3-positive autophagosomes in hypoxia.** (A) HEK-293 cells expressing WT Atg9A or the S761A mutant or that were mock transfected were treated with hypoxia for 12 h with or without 100 nM bafilomycin A1. Cells were lysed and immunoblotted for endogenous LC3-I and LC3-II. The intensity of LC3 bands was quantified by Li-Cor infrared imaging in order to determine the LC3-II/LC3-I ratio. The combined results from five separate experiments are shown in the bar graph with means ± standard errors. (B) U2OS cells infected with Golgi-GFP Bac Mam (Life Technologies, Inc.) were transfected with the RFP-tagged Atg9A WT or S761A mutant and treated with hypoxia or normoxia for 12h. After fixing, cells were analyzed by confocal microscopy. (C) HeLa cells stably expressing GFP-LC3 were transfected with the RFP-tagged Atg9A WT or S761A mutant and treated with hypoxia or normoxia for 12 h. After fixing, cells were analyzed by using confocal microscopy. The panel below the images shows phosphorylation at S761 in hypoxia-treated (12 h) HeLa cells. (D) LC3 punctate structures were counted in RFP-tagged Atg9A WT- or S761A mutant-expressing cells. Means ± standard errors are shown. The statistical significance of the differences between the WT and the S761A mutant was calculated by using two-tailed unpaired Student's t test with equal variance (n = 86 [WT normoxia], n = 76 [S761A mutant normoxia], n = 84 [WT hypoxia], and n = 87 [S761A mutant hypoxia]). *, P value of 1.43E-22. (E) Percentage of GFP-LC3 punctate structures colocalizing with RFP-Atg9A (WT or S761A mutant) determined by manually counting punctate structures in multiple fields (the number of GFP-LC3 and RFP-Atg9A puncta divided by the total number of GFP-LC3 puncta). Means ± standard errors are shown. The statistical significance of the difference between the WT and the S761A mutant was calculated by using two-tailed unpaired Student's t test with equal variance (n = 86 [WT normoxia], n = 76 [S761A mutant normoxia], n = 84 [WT hypoxia], and n = 87 [S761A mutant hypoxia]). *, P value of 3.87E-13.

An intriguing observation from our study is that ULK1 and AMPK are required for basal (nutrient-replete) phosphorylation of Atg9A at S761. It should be noted that Kim et al. found previously that ULK1 activity is inhibited by mTOR under nutrient- replete conditions (48), which seems to conflict with our observation that ULK1 knockdown decreases S761 phosphorylation under basal conditions. However, while data from the in vitro ULK1 kinase assay (Fig. 2-5G) suggest that ULK1 is capable of phosphorylating Atg9A, it is possible that ULK1 is simply part of a complex with AMPK and Atg9A (potentially bridging the interaction with Atg9A) under basal conditions. Indeed, our data do not rule out the possibility the ULK1 plays an ancillary role, independent of its kinase activity, to AMPK in S761 phosphorylation. Consistent with this idea, Shang et al. found that ULK1 and AMPK form a complex that exists only under nutrient-replete conditions and is lost upon starvation (42). Furthermore, the sequence surrounding S761 forms a canonical AMPK motif but does not exactly conform to known ULK1 phosphorylation motifs, which often possess a hydrophobic residue at the -3 position (as opposed to the positively charged arginine near S761) (41). In addition, Mack et al. found that the ULK1 protein is required for Atg9A cycling under nutrient-replete conditions but not under starved conditions, an observation that might be explained by ULK1-mediated control of basal S761 phosphorylation (39). Future work will determine whether ULK1 is acting in parallel or in cooperation with AMPK to mediate S761 phosphorylation.

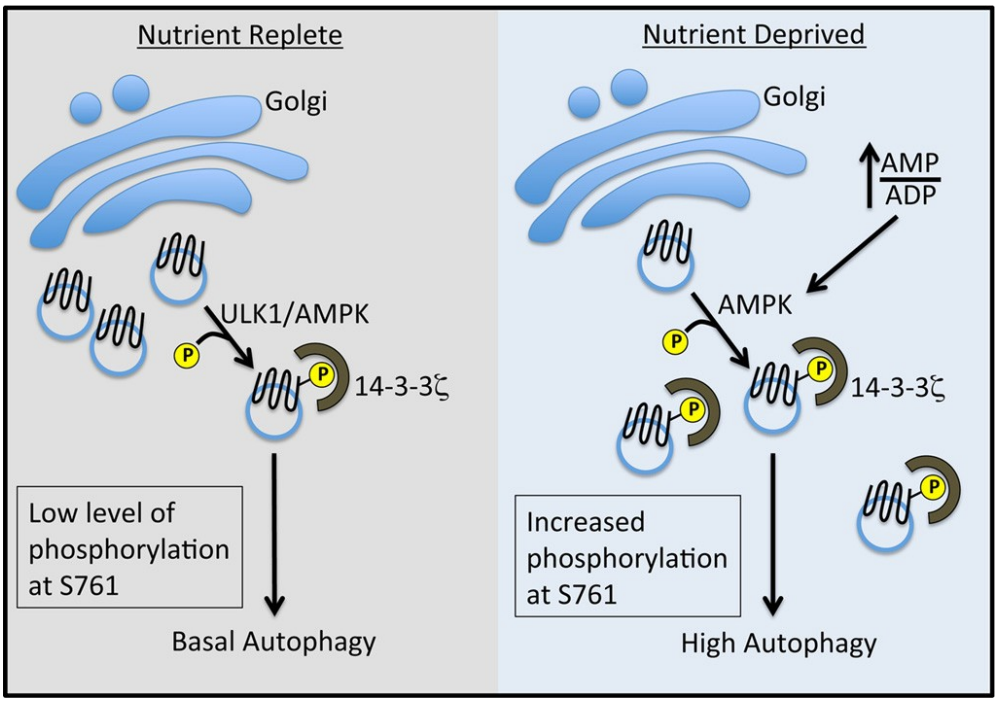

Figure 2-7 **Model of ULK1- and AMPK-mediated regulation of Atg9A via phosphorylation at S761.** Under nutrient-replete conditions, a low level of phosphorylation is dependent on ULK1 and AMPK, suggesting a relationship between these kinases under basal conditions (42). We favor the hypothesis that AMPK is directly responsible for Atg9A phosphorylation, with ULK1 playing an ancillary role (see Discussion). We posit that this low level of phosphorylation maintains a basal level of autophagy. Under nutrient deprivation, an increased AMP-to-ADP ratio results in the full activation of AMPK and in- creased phosphorylation at S761 independent of ULK1, leading to increased autophagy, localization of Atg9A to autophagosomes, and autophagosome biogenesis.

A recent study by Papinski and colleagues found that Atg1 (ULK1) directly phosphorylates yeast Atg9A at multiple Serines within its cytoplasmic C-terminal region (41). Those authors also observed that nonphosphorylatable mutants of Atg9A were un-able to localize to autophagosomes. The similarity between their observations and our data suggests that the ULK1-Atg9A link is conserved. However, there is very little sequence conservation between yeast and mammalian Atg9A, and we found no sequence in yeast Atg9A with even remote similarity to the motif surrounding S761. Thus, it is possible that the role of phosphorylation within the C-terminal region of Atg9A is functionally conserved between yeast and mammals but that regulation of mammalian Atg9A phosphorylation has been coopted by AMPK during nutrient stress.

This study also sheds light on the dynamic role of 14-3-3ζ in promoting the adaptation of cells to stress and highlights the potential of 14-3-3 interactomics to identify novel phosphorylation- based regulatory mechanisms involved in the stress response. Based on our observations, in addition to work by other groups (31, 32, 50), it is clear that the 14-3-3ζ interactome is highly context dependent. For example, in contrast to 14-3-3ζ mediated Atg9 activation in hypoxia, 14-3-3ζ was reported to interact with the class III PI3K human vacuolar sorting protein 34 (hVps34) to suppress autophagy under glucose-fed conditions (51). Conversely, amino acid withdrawal induces an interaction between 14-3-3ζ and Raptor (which we also detected in our hypoxic proteomics experiments), a component of the mTOR complex, which leads to Raptor sequestration, mTOR inhibition, and activation of autophagy (36). Other studies have highlighted a role for 14-3-3 in the regulation of glucose receptor trafficking in response to insulin (31, 52, 53). Thus, 14-3-3ζ, acting dynamically at multiple levels, promotes a prosurvival cellular program appropriate for the changing physiological conditions of the cell.

In summary, our data show that hypoxic conditions trigger a rearrangement of the 14-3-3ζ interactome. These experiments led to the discovery of a novel mechanism of autophagy regulation via phosphorylation of mammalian Atg9A. While our data indicate that S761 phosphorylation is required for the Atg9A-mediated growth of autophagosomes and Atg9A colocalization with LC3-positive autophagosomal structures, several important questions remain. At which step in the Atg9A trafficking pathway does S761 phosphorylation occur? Does S761 phosphorylation/14-3-3ζ binding orchestrate an interaction between Atg9A and proteins known to mediate Atg9A trafficking or the release of Atg9A from a membrane (e.g., endoplasmic reticulum, Golgi, or endosomal) tether? Moreover, is there an opposing mechanism to dampen AMPK-induced S761

phosphorylation, such as phosphatase activation, to avoid excessive autophagy? Answers to these questions will surely add more pieces to the complex puzzle of autophagy regulation in mammals.

2.5 Materials and Method

2.5.1 Cell culture and transfection.

HEK-293 cells and U2OS cells were cultured in Dulbecco's modified Eagle's medium (DMEM) supplemented with 10% fetal bovine serum (FBS) at 37°C in a 5% CO_2 incubator. HeLa cells stably expressing green fluorescent autophagy reporter protein GFP- LC3, kindly provided by Beth Levine at the University of Texas Southwestern Medical Center (18), were cultured in DMEM supplemented with 10% FBS at 37°C in a 5% CO_2 incubator. For all hypoxia treatments, cells were treated in glucose-free DMEM supplemented with 2 mM glucose and 10% dialyzed FBS (Invitrogen) at 37°C in a 1% O_2 incubator. HEK- 293 cells, U2OS cells, and HeLa cells were transiently transfected with red fluorescent protein (RFP)-Atg9A, hemagglutinin (HA)-Atg9A, HA–14-3- 3ζ, and/or AMPK alpha2 K45R (Addgene plasmid number 15992) plasmids by using FuGENE6 (Promega), TurboFect (Thermo Scientific), or polyethylenimine (PEI) (Polyscience, Inc.) according to the manufacturer's protocols.

2.5.2 Antibodies and chemicals.

The following antibodies were used. Anti-HA (F-7), anti-FLAG (D-8), anti-14-3-3ζ (C-16), anti-actin R (I-19), and anti-kinesin (H-50) were purchased from Santa Cruz Biotechnology. Antibodies for phospho-acetyl coenzyme A (acetyl-CoA) carboxylase (catalog number 3661), phospho-Thr172 of AMPK α1 (catalog number 2535), LC3B (catalog number 2775S), ULK1 (catalog number 8054S), the phosphoserine 14-3-3ζ motif ("pMotif") (9601S), Atg9A (catalog number 9730S), and AS160 (catalog number 2447S)

were purchased from Cell Signaling. Antibodies for AMPK α1 and AMPK α2 were custom made by Affinity BioReagents. Anti-ULK2 (catalog number ab56736) was purchased from Abcam.

The following inhibitors were used. Complete protease inhibitors were purchased from Roche and used according to the manufacturer's procedures. SB203580 (catalog number 13067), Dynasore (catalog number 14062), wortmannin (catalog number 10010591), and bafilomycin A1 (catalog number 11038) were purchased from Cayman Chemicals. Compound C (catalog number 171260) and UCN-01 (catalog number 539644) were purchased from Calbiochem. Site-directed mutagenesis kits (catalog number 200521-5) were purchased from Agilent Technologies. The ULK1 enzyme system (catalog number U3521) was purchased from Promega. For *in vitro* AMPK assays, *in vitro* kinase assay buffer, recombinant α1–2/β1–2 AMPK (rAMPK) heterotrimers, and liver kinase B1 (LKB1)-STRAD-MO25 (catalog number 14-596) were purchased from Upstate-Millipore. Cell Light Golgi-GFP Bac Mam 2.0 (catalog number C10592) was purchased from Life Technologies. A Lambda phosphatase enzyme kit (catalog number P0753S) was purchased from New England BioLabs, Inc.

2.5.3 Plasmids

14-3-3ζ-HA was cloned into pCDNA3.1. Atg9A-HA and Atg9A-RFP plasmids were kindly provided by Sharon Tooze, London Research Institute, United Kingdom. The dominant negative pAMPK alpha2 K45R construct was purchased from Addgene (catalog number 15992).

2.5.4 RNA interference.

ULK1 small interfering RNA (siRNA) (catalog number M-005049-00) and PRKAA1 siRNA (catalog number M-005027-02) were purchased from Thermo Scientific (Dharmacon siGENOME SMARTpool). ULK2 siRNA (catalog number 956) and PRKAA2 siRNA (catalog number 103599) were purchased from Ambion by Life Technologies, Inc. siRNA was transfected by using Lipofectamine RNAiMAX (Life Technologies) at a 66 nM or 100 nM final concentration, according to the manufacturer's instructions.

2.5.5 Immunoprecipitation and immunoblotting.

To prepare whole-cell extracts, cells were washed twice and harvested with ice-cold phosphate – buffered saline (PBS). Cell pellets were resuspended in either coimmunoprecipitation (co-IP) buffer (10 mM HEPES [pH 7.5], 150 mM KCl, 0.1% NP-40) or Atg9A lysis buffer (20 mM Tris-HCl [pH 7.5], 150 mM NaCl, 0.3% [wt/vol] Triton X-100, and 5 mM EDTA) supplemented with protease and phosphatase inhibitors and incubated for 15 min on ice or at 4°C with gentle rotation. Lysates were syringed through a 25-gauge needle 10 times and centrifuged at 21,000 rpm for 10 min at 4°C. For coimmunoprecipitation of 14-3-3ζ with Atg9A-HA or Atg9A with 14-3-3 ζ –HA, lysates of cells transfected with Atg9A-HA or 14-3-3 ζ –HA were incubated with anti-HA–agarose beads for1h at 4°C with gentle rotation. The beads were then washed once with lysis buffer and three times with cold PBS. The coimmunoprecipitated proteins were eluted with modified Laemmli sample buffer by boiling at 100°C for 5 min. The proteins were analyzed followed by immunoblotting using infrared fluorescent secondary antibodies and a Li-Cor Odyssey imaging system.

2.5.6 *In vitro* kinase assay.

rAMPK heterotrimers were prepared as described previously (19). Activation of 4 µg rAMPK was accomplished by incubation for 60 min at 30°C with 0.1 µg recombinant LKB1-STRAD- MO25 (catalog number 14-596; Upstate-Millipore) in 25 µl of kinase reaction buffer (40 mM HEPES, 0.2 mM AMP, 80 mM NaCl, 8% glycerol, 0.8 mM EDTA, 0.8 mM dithiothreitol [DTT], 5 mM $MgCl_2$, 0.2 mM ATP [pH

7.0]). The immunoprecipitated Atg9A-HA on anti-HA–agarose beads was incubated with Lambda phosphatase (400 U) for 10 min at 30°C. The beads were then washed three times with ice-cold PBS and incubated with the *in vitro* kinase reaction buffer (40 mM HEPES, 0.2 mM AMP, 80 mM NaCl, 8% glycerol, 0.8 mM EDTA, 0.8 mM DTT, 5 mM $MgCl_2$, 0.2 mM ATP [pH 7.0]) containing LKB1, activated AMPK with LKB1, or ULK1 for 30 min at 30°C. The proteins were eluted with modified Laemmli sample buffer by boiling at 100°C for 5 min and analyzed, followed by immunoblotting using infrared fluorescent secondary antibodies and the Li-Cor Odyssey imaging system.

2.5.7 Inhibitor assays.

The following inhibitors and concentrations were used in cell assays: LY294002 at 50 μM; UCN01 at 1 μM, 500 nM, and 300 nM; compound C at 20 μM; SB203580 at 2 μM; and U0126 at 20 μM.

2.5.8 Immunostaining and confocal microscopy.

Cells were seeded into 6-well plates on collagenized glass coverslips and allowed to grow overnight. Following transfection of Atg9A-RFP and/or infection with Cell Light Golgi- GFP Bac Mam 2.0 (catalog number C10592), cells were washed three times with PBS. Cells were then fixed in 4% paraformaldehyde in PBS for 15 min with light agitation at room temperature. Following fixing cells were washed three times with PBS and then permeabilized and blocked for 30 min with 1% whole goat serum in 0.1% Tween in PBS (0.1% PBS-T). Following permeabilization and blocking, 4-6-diamidino-2-phenylindole (DAPI) (Molecular Probes) was added for 30 min in 0.1% PBS-T with light agitation at room temperature. Following secondary antibody incubation, cells were washed three times for 10 min with PBS and mounted onto slides with Pro- Long Gold Antifade reagent (Molecular Probes). Micrographs were taken with an Olympus FluoView FV1000 confocal laser scanning microscope mounted on an Olympus IX81 inverted microscope with an oil-immersed 60X objective. Sequential scans were taken with consistent fixed settings for DAPI, GFP, and RFP.

2.5.9 Gel filtration assay.

Cells transfected with HA–14-3-3ζ were treated with normoxia or hypoxia for 4 h before lysis by Dounce homogenization in hypotonic lysis buffer (20 mM HEPES [pH 7.5], 10 mM KCl, 1.5 mM $MgCl_2$, 1 mM EDTA, 1 mM EGTA, 1 mM DTT, and 5 μg/ml each aprotinin and leupeptin). Lysates were centrifuged at 4°C for 15 min at 13,200 rpm, and the protein concentration of the supernatant was determined by using the Bio-Rad protein assay reagent. Five hundred microliters of 8 mg/ml of lysates was loaded onto a Superdex 200 column at a flow rate of 0.3 ml/min to collect fractions.

2.5.10 Mass spectrometry to identify interacting partners.

HA- tagged 14-3-3ζ (or mock control) coimmunoprecipitates were digested in solution after normalization to equivalent total protein concentrations by using a mini-Bradford assay (Bio-Rad, Inc.). Briefly, samples were supplemented with 0.25% Rapigest SF (Waters Corp.) in 50 mM ammonium bicarbonate (AmBic) and then reduced at 80°C with 20 mM dithiothreitol, followed by alkylation at room temperature with 40 mM iodoacetamide. Finally, digestion with trypsin (sequencing grade, modified; Promega) was performed overnight at 37°C (50:1 substrate/enzyme ratio). Digestion was quenched and Rapigest was degraded by using acidification to 1% (vol/vol) trifluoroacetic acid (TFA) for2h at 60°C. Finally, samples were dried and resuspended at 1 mg/ml in 200 mM ammonium formate (pH 10) for analysis by two-dimensional liquid chromatography-tandem mass spectrometry (LC/LC-MS/MS).

2.5.11 Multidimensional LC-MS/MS.

Three microliters of peptide sample digests was analyzed by using a nanoAcquity UPLC system with 2D Technology coupled to a Synapt G2 HDMS mass spectrometer (Waters Corp., Milford, MA), using a method that generated five fractions at pH 10 with approximately equal loading in each fraction, which was similar to methods described previously (20–22). The sample was first trapped at 2 μl/ min at a 97/3 (vol/vol) water/methyl cyanide (MeCN) ratio in 20 mM ammonium formate (pH 10) on a 5-μm XBridge

BEH130 C18 300-µm by 50-mm column. Two minute steps at 2 µl/min to the following percentages of MeCN were used to generate the 5 fractions at pH 10, with the composition returning to 97/3/0.1 during the analytical second dimension: 10.8%, 14.0%, 16.7%, 20.4%, and 50.0%. At each fraction step, the flow through from the first dimension was diluted online 10-fold with a 99.8/0.1/0.1 (vol/vol/vol) ratio of water/MeCN/formic acid and trapped on a 5-µm Symmetry C18 300-µm by 180-mm trapping column. Separations for each fraction were then performed on a 1.7-µm Acquity BEH130 C18 75-µm by 150-mm column (Waters), using a 37-min gradient of 7 to 35% acetonitrile with 0.1% formic acid at a flow rate of 0.5 µl/min and a 35°C column temperature. We conducted one five-fraction data-independent analysis using ion mobility high-definition mass spectrometry (HDMSE) analysis and one five-fraction traditional data-dependent analysis (DDA). The HDMSE runs used a 0.6-s cycle time, alternating between low collision energy (6-V) and a high-collision-energy ramp in the transfer region (27 to 50 V). The DDA mode utilized a 0.6-s MS scan followed by MS/MS acquisition on the top three ions with charges of >1. MS/MS scans for each ion used an isolation window of approximately 2.3 Da, 0.6-s scans with a maximum of 3 s per precursor, and dynamic exclusion for 120 s within 1.2 Da of the selected precursor *m/z*.

2.5.12 LC-MS data processing and quantitation.

The data were searched against the UNIPROT database with *Homo sapiens* taxonomy and reviewed status (http://www.uniprot.org/). The database was appended with several common contaminant or internal standard proteins (ALBU_BOVIN, ADH1_YEAST, ENO1_YEAST, PYGM_RABIT, and CASA1_

BOVIN) and a 1X reverse database for peptide false-discovery-rate determination. MS/MS spectra generated by DDA were compiled into .mgf format by using Mascot Distiller v2.2 and submitted to the Mascot v2.2 (Matrix Sciences, Inc.) search engine. For HDMSE and MSE data, Protein- Lynx Global Server 2.5 (Waters Corp.) was used to generate searchable files, which were then submitted to the IdentityE search engine (Waters Corp., Milford, MA). The automated merge function within PLGS 2.5 was used to

combine spectral information from each of the five fractions prior to searches with IdentityE. The precursor ion mass tolerances were 10 ppm and 5 ppm for Mascot and PLGS searches, respectively, and the product ion tolerances were 0.04 Da for Mascot and 13 ppm for PLGS. For both search engines, the enzyme specificity was set to tryptic, and a maximum of 2 missed cleavages were allowed. Carbamidomethyl cysteine was included as a fixed modification, and variable modifications included oxidized methionine, deamidated asparagine and glutamine, acetylated lysine, and phosphorylated serine and threonine. PLGS searches were performed by requiring at least 3 products per precursor, 7 product ions per protein, and 1 peptide per protein. Qualitative data were curated in Scaffold v4 (Proteome Software, Inc.). Relative quantitation between hypoxia and normoxia conditions was performed based on first analyzer (MS1) extracted-ion chromatograms by using the Skyline v2.5.1 software environment (23). The raw data associated with this analysis are available on the Panorama server (http://goo.gl/aO68ge).

2.5.13 Detection of hypoxia-induced phosphorylation of Atg9A by LC-MS/ MS.

HA-Atg9A immunoprecipitates were prepared for mass spectrometry by using a modified version of filter-aided sample preparation (24). Briefly, HA-tagged Atg9A was overexpressed and immunoprecipitated from HEK-293 cells. Next, it was reduced with dithiothreitol (DL; Sigma- Aldrich) and alkylated with iodoacetamide (BioUltra; Sigma-Aldrich). It was then digested on the filter in 50 mM ammonium bicarbonate (ReagentPlus; Sigma-Aldrich) for 5 to 6 h with 0.1 µg trypsin (sequencing grade; Promega). Samples were acidified with formic acid (Optima; Fisher Scientific) to 1% (vol/vol) prior to mass spectral analysis.

Mass spectrometry was performed by using an LTQ Orbitrap XL mass spectrometer with the following parameters. Peptides were eluted over a 90-min H_2O–acetonitrile– 0.1% formic acid gradient flowing at 325 µl/ min by using the Eksigent NanoLC Ultra instrument with a Waters Peptide Separation Technology C18 column. MS1 scans were analyzed at a resolution setting of 60,000 (at 400 *m/z*) with the Orbitrap

instrument. The top 10 most abundant precursor ions were subject to multistage activation in the LTQ mass spectrometer with neutral loss masses corresponding to a phosphate loss (32.66, 48.99, and 97.97 Da) (25). Dynamic exclusion was used with a 180-s exclusion duration.

Data analysis was performed with Mascot, PhosphoRS 3.0, and Percolator by using the Proteome Discoverer version 1.4 software package (26– 28). Precursor mass tolerances were set to 10 ppm, and fragment mass tolerances were set to 0.8 Da. Carbomethylation (C), oxidation (M), and phosphorylation (STY) were set as dynamic modifications. We allowed up to 2 missed trypsin cleavages and searched against the UNI_Human database. A strict false discovery rate was set by using a Percolator *q*-value threshold of 0.01. Additionally, PhosphoRS 3.0 phosphorylation site localization software assigned S761 a posttranslational modifi (PTM) score of 76.6, whereas other potential phosphorylation sites on the same peptide had a PTM score of <12

2.6 References

1. **Chen, S., S. Synowsky, M. Tinti, and C. MacKintosh.** 2011. The capture of phosphoproteins by 14-3-3 proteins mediates actions of insulin. Trends in endocrinology and metabolism: TEM **22:**429-436.
2. **Datta, S. R., A. Katsov, L. Hu, A. Petros, S. W. Fesik, M. B. Yaffe, and M. E. Greenberg.** 2000. 14-3-3 proteins and survival kinases cooperate to inactivate BAD by BH3 domain phosphorylation. Molecular cell **6:**41-51.
3. **Davies, S. P., H. Reddy, M. Caivano, and P. Cohen.** 2000. Specificity and mechanism of action of some commonly used protein kinase inhibitors. The Biochemical journal **351:**95-105.
4. **DeYoung, M. P., P. Horak, A. Sofer, D. Sgroi, and L. W. Ellisen.** 2008. Hypoxia regulates TSC1/2-mTOR signaling and tumor suppression through REDD1-mediated 14-3-3 shuttling. Genes & development **22:**239-251.
5. **Dubois, F., F. Vandermoere, A. Gernez, J. Murphy, R. Toth, S. Chen, K. M. Geraghty, N. A. Morrice, and C. MacKintosh.** 2009. Differential 14-3-3 affinity capture reveals new downstream targets of phosphatidylinositol 3-kinase signaling. Molecular & cellular proteomics : MCP **8:**2487-2499.
6. **Egan, D. F., D. B. Shackelford, M. M. Mihaylova, S. Gelino, R. A. Kohnz, W. Mair, D. S. Vasquez, A. Joshi, D. M. Gwinn, R. Taylor, J. M. Asara, J. Fitzpatrick, A. Dillin, B. Viollet,**

M. Kundu, M. Hansen, and R. J. Shaw. 2011. Phosphorylation of ULK1 (hATG1) by AMP-activated protein kinase connects energy sensing to mitophagy. Science **331:**456-461.

7. **Fan, Y., J. W. Thompson, L. G. Dubois, M. A. Moseley, and J. J. Wernegreen.** 2013. Proteomic analysis of an unculturable bacterial endosymbiont (Blochmannia) reveals high abundance of chaperonins and biosynthetic enzymes. Journal of proteome research **12:**704-718.

8. **Gardino, A. K., and M. B. Yaffe.** 2011. 14-3-3 proteins as signaling integration points for cell cycle control and apoptosis. Seminars in cell & developmental biology **22:**688-695.

9. **Gwinn, D. M., D. B. Shackelford, D. F. Egan, M. M. Mihaylova, A. Mery, D. S. Vasquez, B. E. Turk, and R. J. Shaw.** 2008. AMPK phosphorylation of raptor mediates a metabolic checkpoint. Molecular cell **30:**214-226.

10. **He, C., M. Baba, Y. Cao, and D. J. Klionsky.** 2008. Self-interaction is critical for Atg9A transport and function at the phagophore assembly site during autophagy. Molecular biology of the cell **19:**5506-5516.

11. **Hoos, M. D., B. M. Richardson, M. W. Foster, A. Everhart, J. W. Thompson, M. A. Moseley, and C. A. Colton.** 2013. Longitudinal study of differential protein expression in an Alzheimer's mouse model lacking inducible nitric oxide synthase. Journal of proteome research **12:**4462-4477.

12. **Hu, Y. L., M. DeLay, A. Jahangiri, A. M. Molinaro, S. D. Rose, W. S. Carbonell, and M. K. Aghi.** 2012. Hypoxia-induced autophagy promotes tumor cell survival and adaptation to antiangiogenic treatment in glioblastoma. Cancer research **72:**1773-1783.

13. **Inoki, K., T. Zhu, and K. L. Guan.** 2003. TSC2 mediates cellular energy response to control cell growth and survival. Cell **115:**577-590.

14. **Kall, L., J. D. Canterbury, J. Weston, W. S. Noble, and M. J. MacCoss.** 2007. Semi-supervised learning for peptide identification from shotgun proteomics datasets. Nature methods **4:**923-925.

15. **Kim, J., M. Kundu, B. Viollet, and K. L. Guan.** 2011. AMPK and mTOR regulate autophagy through direct phosphorylation of Ulk1. Nature cell biology **13:**132-141.

16. **Komander, D., G. S. Kular, J. Bain, M. Elliott, D. R. Alessi, and D. M. Van Aalten.** 2003. Structural basis for UCN-01 (7-hydroxystaurosporine) specificity and PDK1 (3-phosphoinositide-dependent protein kinase-1) inhibition. The Biochemical journal **375:**255-262.

17. **Lee, J. W., S. Park, Y. Takahashi, and H. G. Wang.** 2010. The association of AMPK with ULK1 regulates autophagy. PloS one **5:**e15394.

18. **Li, Y., L. Zou, Q. Li, B. Haibe-Kains, R. Tian, Y. Li, C. Desmedt, C. Sotiriou, Z. Szallasi, J. D. Iglehart, A. L. Richardson, and Z. C. Wang.** 2010. Amplification of LAPTM4B and YWHAZ contributes to chemotherapy resistance and recurrence of breast cancer. Nature medicine **16:**214-218.

19. **Li, Z., J. Zhao, Y. Du, H. R. Park, S. Y. Sun, L. Bernal-Mizrachi, A. Aitken, F. R. Khuri, and H. Fu.** 2008. Down-regulation of 14-3-3 eta suppresses anchorage-independent growth of lung cancer cells through anoikis activation. Proceedings of the National Academy of Sciences of the United States of America **105:**162-167.

20. **Lu, J., H. Guo, W. Treekitkarnmongkol, P. Li, J. Zhang, B. Shi, C. Ling, X. Zhou, T. Chen, P. J. Chiao, X. Feng, V. L. Seewaldt, W. J. Muller, A. Sahin, M. C. Hung, and D. Yu.** 2009. 14-3-3 eta Cooperates with ErbB2 to promote ductal carcinoma in situ progression to invasive breast cancer by inducing epithelial-mesenchymal transition. Cancer cell **16:**195-207.

21. **Lynn, E. G., C. J. McLeod, J. P. Gordon, J. Bao, and M. N. Sack.** 2008. SIRT2 is a negative regulator of anoxia-reoxygenation tolerance via regulation of 14-3-3 zeta and BAD in H9c2 cells. FEBS letters **582:**2857-2862.

22. **Mack, H. I., B. Zheng, J. M. Asara, and S. M. Thomas.** 2012. AMPK-dependent phosphorylation of ULK1 regulates ATG9A localization. Autophagy **8:**1197-1214.

23. **MacLean, B., D. M. Tomazela, N. Shulman, M. Chambers, G. L. Finney, B. Frewen, R. Kern, D. L. Tabb, D. C. Liebler, and M. J. MacCoss.** 2010. Skyline: an open source document editor for creating and analyzing targeted proteomics experiments. Bioinformatics **26:**966-968.

24. **Matta, A., K. M. Siu, and R. Ralhan.** 2012. 14-3-3 zeta as novel molecular target for cancer therapy. Expert opinion on therapeutic targets.

25. **Maxwell, S. A., Z. Li, D. Jaye, S. Ballard, J. Ferrell, and H. Fu.** 2009. 14-3-3 eta mediates resistance of diffuse large B cell lymphoma to an anthracycline-based chemotherapeutic regimen. The Journal of biological chemistry **284:**22379-22389.

26. **Mizushima, N., T. Yoshimori, and B. Levine.** 2010. Methods in mammalian autophagy research. Cell **140:**313-326.

27. **Neal, C. L., J. Yao, W. Yang, X. Zhou, N. T. Nguyen, J. Lu, C. G. Danes, H. Guo, K. H. Lan, J. Ensor, W. Hittelman, M. C. Hung, and D. Yu.** 2009. 14-3-3 eta overexpression defines high risk for breast cancer recurrence and promotes cancer cell survival. Cancer research **69:**3425-3432.

28. **Neal, C. L., and D. Yu.** 2010. 14-3-3 eta as a prognostic marker and therapeutic target for cancer. Expert opinion on therapeutic targets **14:**1343-1354.

29. **Neukamm, S. S., R. Toth, N. Morrice, D. G. Campbell, C. Mackintosh, R. Lehmann, H. U. Haering, E. D. Schleicher, and C. Weigert.** 2012. Identification of the amino acids 300-600 of IRS-2 as 14-3-3 binding region with the importance of IGF-1/insulin-regulated phosphorylation of Ser-573. PloS one **7:**e43296.

30. **Nishimura, Y., S. Komatsu, D. Ichikawa, H. Nagata, S. Hirajima, H. Takeshita, T. Kawaguchi, T. Arita, H. Konishi, K. Kashimoto, A. Shiozaki, H. Fujiwara, K. Okamoto, H. Tsuda, and E. Otsuji.** 2013. Overexpression of YWHAZ relates to tumor cell proliferation and malignant outcome of gastric carcinoma. British journal of cancer **108:**1324-1331.

31. **Nutt, L. K., M. R. Buchakjian, E. Gan, R. Darbandi, S. Y. Yoon, J. Q. Wu, Y. J. Miyamoto, J. A. Gibbons, J. L. Andersen, C. D. Freel, W. Tang, C. He, M. Kurokawa, Y. Wang, S. S. Margolis, R. A. Fissore, and S. Kornbluth.** 2009. Metabolic control of oocyte apoptosis mediated by 14-3-3 eta-regulated dephosphorylation of caspase-2. Dev Cell **16:**856-866.

32. **Orsi, A., M. Razi, H. C. Dooley, D. Robinson, A. E. Weston, L. M. Collinson, and S. A. Tooze.** 2012. Dynamic and transient interactions of Atg9A with autophagosomes, but not membrane integration, are required for autophagy. Molecular biology of the cell **23:**1860-1873.

33. **Papinski, D., M. Schuschnig, W. Reiter, L. Wilhelm, C. A. Barnes, A. Maiolica, I. Hansmann, T. Pfaffenwimmer, M. Kijanska, I. Stoffel, S. S. Lee, A. Brezovich, J. H. Lou, B.**

E. Turk, R. Aebersold, G. Ammerer, M. Peter, and C. Kraft. 2014. Early steps in autophagy depend on direct phosphorylation of Atg9A by the Atg1 kinase. Molecular cell **53:**471-483.

34. **Perkins, D. N., D. J. Pappin, D. M. Creasy, and J. S. Cottrell.** 1999. Probability-based protein identification by searching sequence databases using mass spectrometry data. Electrophoresis **20:**3551-3567.

35. **Pozuelo Rubio, M., K. M. Geraghty, B. H. Wong, N. T. Wood, D. G. Campbell, N. Morrice, and C. Mackintosh.** 2004. 14-3-3-affinity purification of over 200 human phosphoproteins reveals new links to regulation of cellular metabolism, proliferation and trafficking. The Biochemical journal **379:**395-408.

36. **Pozuelo-Rubio, M.** 2010. Proteomic and biochemical analysis of 14-3-3-binding proteins during C2-ceramide-induced apoptosis. The FEBS journal **277:**3321-3342.

37. **Pozuelo-Rubio, M.** 2011. Regulation of autophagic activity by 14-3-3 eta proteins associated with class III phosphatidylinositol-3-kinase. Cell death and differentiation **18:**479-492.

38. **Puri, C., M. Renna, C. F. Bento, K. Moreau, and D. C. Rubinsztein.** 2013. Diverse autophagosome membrane sources coalesce in recycling endosomes. Cell **154:**1285-1299.

39. **Reggiori, F., and S. A. Tooze.** 2012. Autophagy regulation through Atg9A traffic. The Journal of cell biology **198:**151-153.

40. **Saka, H. A., J. W. Thompson, Y. S. Chen, Y. Kumar, L. G. Dubois, M. A. Moseley, and R. H. Valdivia.** 2011. Quantitative proteomics reveals metabolic and pathogenic properties of Chlamydia trachomatis developmental forms. Molecular microbiology **82:**1185-1203.

41. **Samokhvalov, V., B. A. Scott, and C. M. Crowder.** 2008. Autophagy protects against hypoxic injury in C. elegans. Autophagy **4:**1034-1041.

42. **Schroeder, M. J., J. Shabanowitz, J. C. Schwartz, D. F. Hunt, and J. J. Coon.** 2004. A neutral loss activation method for improved phosphopeptide sequence analysis by quadrupole ion trap mass spectrometry. Analytical chemistry **76:**3590-3598.

43. **Shang, L., S. Chen, F. Du, S. Li, L. Zhao, and X. Wang.** 2011. Nutrient starvation elicits an acute autophagic response mediated by Ulk1 dephosphorylation and its subsequent dissociation from AMPK. Proceedings of the National Academy of Sciences of the United States of America **108:**4788-4793.

44. **Song, J., Z. Qu, X. Guo, Q. Zhao, X. Zhao, L. Gao, K. Sun, F. Shen, M. Wu, and L. Wei.** 2009. Hypoxia-induced autophagy contributes to the chemoresistance of hepatocellular carcinoma cells. Autophagy **5:**1131-1144.

45. **Taus, T., T. Kocher, P. Pichler, C. Paschke, A. Schmidt, C. Henrich, and K. Mechtler.** 2011. Universal and confident phosphorylation site localization using phosphoRS. Journal of proteome research **10:**5354-5362.

46. **Taylor, E. B., W. J. Ellingson, J. D. Lamb, D. G. Chesser, C. L. Compton, and W. W. Winder.** 2006. Evidence against regulation of AMP-activated protein kinase and LKB1/STRAD/MO25 activity by creatine phosphate. American journal of physiology. Endocrinology and metabolism **290:**E661-669.

47. **Wang, Z., W. A. Wilson, M. A. Fujino, and P. J. Roach.** 2001. Antagonistic controls of autophagy and glycogen accumulation by Snf1p, the yeast homolog of AMP-activated protein kinase, and the cyclin-dependent kinase Pho85p. Molecular and cellular biology **21:**5742-5752.

48. **Webber, J. L., and S. A. Tooze.** 2010. Coordinated regulation of autophagy by p38alpha MAPK through mAtg9A and p38IP. The EMBO journal **29:**27-40.

49. **Wei, Y., Z. Zou, N. Becker, M. Anderson, R. Sumpter, G. Xiao, L. Kinch, P. Koduru, C. S. Christudass, R. W. Veltri, N. V. Grishin, M. Peyton, J. Minna, G. Bhagat, and B. Levine.** 2013. EGFR-Mediated Beclin 1 Phosphorylation in Autophagy Suppression, Tumor Progression, and Tumor Chemoresistance. Cell **154:**1269-1284.

50. **Wilkinson, S., J. O'Prey, M. Fricker, and K. M. Ryan.** 2009. Hypoxia-selective macroautophagy and cell survival signaled by autocrine PDGFR activity. Genes & development **23:**1283-1288.

51. **Wilson, W. R., and M. P. Hay.** 2011. Targeting hypoxia in cancer therapy. Nature reviews. Cancer **11:**393-410.

52. **Wisniewski, J. R., A. Zougman, N. Nagaraj, and M. Mann.** 2009. Universal sample preparation method for proteome analysis. Nature methods **6:**359-362.

53. **Yang, X., W. Cao, L. Zhang, W. Zhang, X. Zhang, and H. Lin.** 2012. Targeting 14-3-3 eta in cancer therapy. Cancer gene therapy **19:**153-159.

54. **Young, A. R., E. Y. Chan, X. W. Hu, R. Kochl, S. G. Crawshaw, S. High, D. W. Hailey, J. Lippincott-Schwartz, and S. A. Tooze.** 2006. Starvation and ULK1-dependent cycling of mammalian Atg9A between the TGN and endosomes. Journal of cell science **119:**3888-3900.

CHAPTER 3 A BioID approach identifies a network of C- and N-terminal Atg9A interactions, including an Atg9A-Atg13-ULK1 complex that acts as a platform for Atg9A C-terminal phosphorylation.

3.1 ABSTRACT

The bulk degradative process of macroautophagy requires the dynamic growth of autophagosomes, which carry cellular contents to the lysosome for recycling. Atg9A, a multi-pass transmembrane protein, is an apical regulator of autophagosome growth, yet its regulatory mechanism remains unclear. Our previous work suggested that the long unstructured C-terminus of Atg9A may be a site of protein docking and regulation. Here we used BioID, along with conventional interactomics, to map the C- and N-terminal proximity-based interactions of Atg9A. We identify a network of Atg9A C-terminal interactions that include members of the ULK1 complex. Using gel filtration, we find that Atg9A co-immunoprecipitates with the ULK1 complex in high molecular weight fractions. Moreover, phosphorylation of the Atg9A C-terminus at S761 appears within the high molecular weight ULK1 complex under nutrient-replete conditions, while hypoxia triggers a redistribution of phosphorylated Atg9A to low molecular weight fractions. Probing these relationships further, we find that Atg13, a component of the ULK1 complex, directly interacts with Atg9A and is required for Atg9A C-terminal phosphorylation. Furthermore, a non-phosphorylatable mutant of Atg9A (S761A) accumulates with Atg13 in high molecular weight complexes. Together, these data suggest that Atg13 recruits Atg9A to the ULK1 complex at the phagophore assemble site (PAS) and that S761 phosphorylation triggers Atg9A retrieval from the PAS.

3.2 INTRODUCTION

The recycling of misfolded proteins, dysfunctional organelles and other molecules through macroautophagy (referred to here as autophagy) is critical for maintaining cellular homeostasis and promoting cell survival during stress. Deregulated autophagy underlies the pathophysiology of many human diseases, including a variety of degenerative disorders, cancer, autoimmunity and infectious disease. The central event in autophagy is the formation of the autophagosome, which begins as a double-membrane cisterna that expands and captures (via random and selective mechanisms) portions of the cytosol and ultimately closes to form a sealed vesicle. The autophagosome fully matures as it fuses with the lysosome, which allows its contents to be degraded and returned to the cell or secreted. The flux of autophagy substrates through this degradative pathway occurs at a low level under basal conditions and increases in response to variety of stresses, including nutrient deprivation and misfolded protein accumulation.

Our understanding of the upstream signaling that controls autophagy mainly derives from studies on nutrient deprivation, in which the opposing activities of AMP-dependent kinase (AMPK) and the mammalian target of rapamycin kinase complex-1 (mTORC1) play a central role. When nutrients are abundant, AMPK and mTORC1 exist in a complex with unc-51-like kinase-1 (ULK1) and its associated proteins (FIP200, ATG13, and ATG101) (1). Under these conditions, active mTORC1 suppresses ULK1 to prevent inappropriately high levels of autophagy (2). As nutrients become depleted, an increase in the AMP-to-ATP ratio activates AMPK, which in turn suppresses mTORC1 (3, 4) and activates ULK1 activity (2, 5-7). This causes mTORC1 and AMPK to dissociate from ULK1, leading to an accumulation of ULK1 puncta on the ER. At these sites, the ULK1 complex activates a VPS34 lipid kinase complex that stimulates synthesis of

phosphatidylinositol 3-phosphate (PI3P) and formation of a membrane precursor to the autophagosome, referred to as the isolation membrane (IM). The location of this emergent autophagosome is called the phagophore assembly site (PAS). Additional autophagy proteins are recruited to the PAS, including conjugation systems that attach the ubiquitin-like protein LC3 to autophagosomes, and ATG9A, the only multi-pass transmembrane protein of the core Atg proteins.

ATG9A, the mammalian homologue of yeast Atg9, contains six transmembrane domains, a long C-terminus and a comparatively short N-terminus. While the transmembrane domains are highly conserved across organisms, the C- and N-terminal regions show very little resemblance between yeast and humans. Studies from yeast and mammalian cells suggest that ATG9A/Atg9 traffics on small membrane vesicles between several membrane compartments (golgi, endosomes, plasma membrane) and the PAS. At the PAS, ATG9A is thought to deposit membrane to support the growing autophagosome, although the mechanism by which this occurs is unclear. Nevertheless, ATG9A is required for the formation of autophagosomes during starvation and mice lacking ATG9A fail to survive the neonatal starvation period, for which autophagy is critical (8, 9). Thus, the mobilization of ATG9A vesicles and their recruitment to the PAS are considered very early steps in autophagy (10).

In general, ATG9A trafficking is partitioned into anterograde (toward the PAS) or retrograde (recycling away from the PAS) trafficking and several factors have been identified as required for each phase. ULK1 is required for anterograde trafficking (11), while FIP200, ATG2A/B and WIPI2 are required for retrograde trafficking (10, 12). In addition, TBC1D14 and TRAPIII control Atg9A trafficking between the endosomal and Golgi compartments (13). However, the

mechanisms by which these factors regulate ATG9A, either directly or indirectly, are not understood.

By using 14-3-3ζ as a tool to understand adaptation to hypoxic stress, we previously identified a phosphorylation at S761 within a conserved 14-3-3ζ docking motif on the C-terminus of ATG9A. The S761A phospho-mutant failed to traffic away from perinuclear sites and cells expressing this mutant showed defective LC3+ autophagosome production in response to hypoxia and glucose starvation. Furthermore, we demonstrated that ULK1 and AMPK coordinately regulate S761 phosphorylation, with AMPK acting as the S761 kinase. Given the binding of 14-3-3ζ and the involvement of ULK1 and AMPK, we posited that the long unstructured (based on modeling predictions) C-terminus of ATG9A serves as a regulatory hub to control ATG9A activity.

In this study we demonstrate that the C-termini of individual ATG9A molecules interact and truncation of the C-terminus alone abrogates ATG9A oligomerization. To probe the N- and C-terminal interactomes of ATG9A, we fused the BirA biotin ligase domain to each end of ATG9A and identified interacting proteins by streptavidin capture and mass spectrometry. This revealed a striking number of C-terminal interacting proteins compared to a relatively small number at the N-terminus. Among the C-terminal interacting proteins were components of the ULK1 complex and the known regulators of retrograde ATG9A trafficking, WIPI2 and ATG2B. Further analysis of these proximity-based interactions under denaturing conditions and by co-IP demonstrated that, of the ULK1 complex proteins, only ATG13 was a direct ATG9A binding partner. Furthermore, using FPLC gel filtration, we found that a large portion of ATG9A co-fractionated with the ~6000 kDa ULK1 complex and co-IPs from pooled fractions confirmed a physical interaction between ATG9A and the ULK1 complex via ATG13. Importantly, FPLC data suggest that under basal conditions, the low level of endogenous phosphorylation at S761 of ATG9A appears within the

ULK1 complex, which includes AMPK. Furthermore, depletion of ATG13 abrogates ATG9A phosphorylation and the non-phosphorylatable ATG9A mutant (S761A) accumulates with ATG13, suggesting that the ATG9A-ULK1 complex interaction is required for S761 phosphorylation. Moreover, upon hypoxia and glucose deprivation, endogenous ATG9A phosphorylation within the ULK1 complex increases and begins to appear in lower molecular weight fractions corresponding in size to the estimated weight of ATG9A vesicles. Together, these data support a model in which the PAS-associated ULK1 complex scaffolds a kinase-substrate interaction between ATG9A and AMPK and that, once phosphorylated, ATG9A is retrieved from the ULK1 complex.

3.3 RESULTS

3.3.1 ATG9A may have a highly unstructured C-terminus region.

Although the structure of ATG9A is not solved, structure prediction tools indicate a highly unstructured C-terminus (Fig 3-1A). Within this putative unstructured region, we previously identified a phosphorylation at S761, which is required for an interaction with 14-3-3ζ (14). Given that 14-3-3ζ typically requires two phosphorylated residues for binding (15) and that a single mutation at the S761 site completely abolished 14-3-3ζ binding, we reasoned that the dimerization or oligomerization of ATG9A may bring two phospho-S761 sites together to create a platform for 14-3-3ζ binding. This idea is supported by the observation that yeast ATG9 oligomerizes via its C termini (16). However, the C-termini of yeast and mammalian ATG9/ATG9A show very little conservation. To test whether mammalian ATG9A also oligomerizes via its C termini, we co-immunoprecipitated (co-IP) a C-terminally truncated form of ATG9A with WT ATG9A using two different affinity tags. As in yeast, mammalian ATG9A shows robust self-oligomerization and loss of the C terminus abolishes this interaction. Our attempts to compare oligomerization of an N-

terminally truncated ATG9A failed as deletion of the N-terminus prevents expression of ATG9A. To get around this issue, we fused the BirA domain of a bacterial biotin ligase (17, 18) to the C-terminal ("ATG9A-BL") or N-terminal ("BL-ATG9A") end of ATG9A and measured these constructs' ability to trans-biotinylate WT ATG9A in cells (constructs shown in Fig 3-1B). Consistent with the co-IP data, ATG9A-BL trans-biotinylated WT ATG9A better than BL-ATG9A (data not shown).

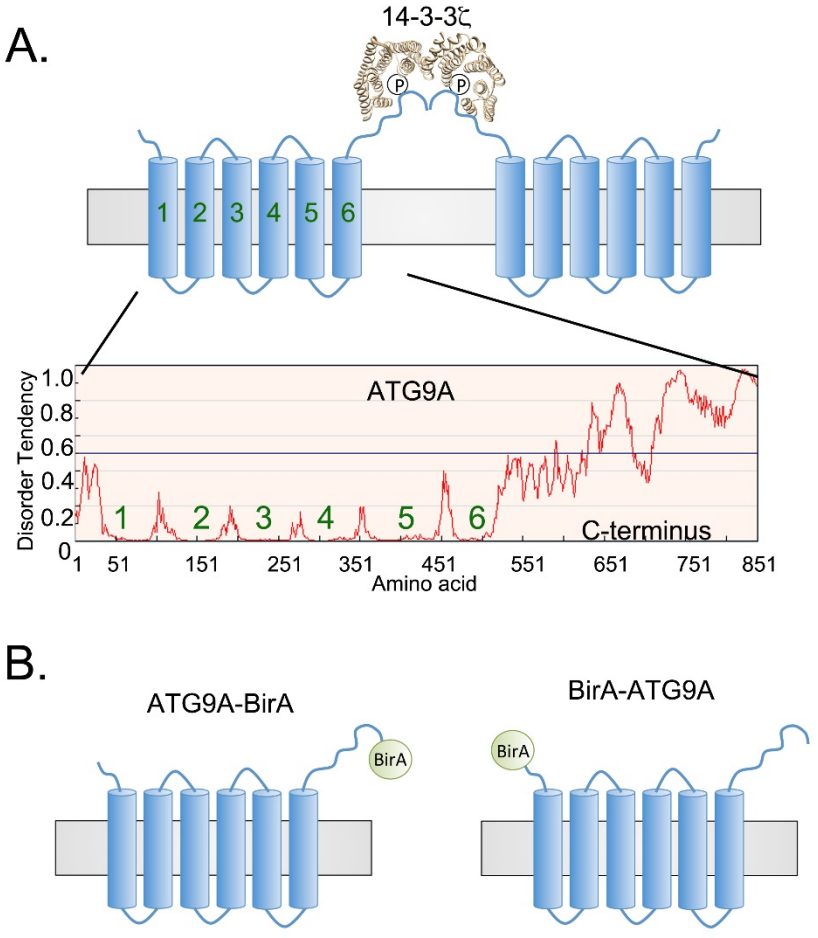

Figure 3-1 **ATG9A has a highly unstructured C-terminus region.** (A) 14-3-3ζ interacts with highly unstructured C – terminus of ATG9A (predicted with 2 independent servers – Dis-EMBL1.5 and IU-Pred). (B) Cartoon diagram of Biotin ligase ATG9A constructs.

3.3.2 A BioID approach identifies the termini specific ATG9A interactomes

These data, in addition to the notion that 14-3-3 proteins are often components of multi-protein complexes, piqued our interest in the possibility that the C-terminus of ATG9A could be a site of protein docking. To test this idea further, we took advantage of the BirA ATG9A constructs and devised a method to identify proximity-based C- and N-terminal ATG9A protein interactions. As shown in figure 3-2A, we expressed the ATG9A-BL and BL-ATG9A constructs in HEK-293 cells supplemented with or without biotin, followed by lysis and pull-down of biotinylated proteins on streptavidin resin. These cells were also treated with or without hypoxia prior to pull-down to see if interactions changed in induced-autophagy conditions. By mass spectrometry, we identified a total of 858 proteins that were only biotinylated in ATG9A-BL or BL-ATG9A expressing cells compared to mock-treated cells (supplemented with biotin but no BL construct). Of these proteins, the majority were biotinylated by the C-terminal ATG9A-BL construct (Fig 3-2B). The biotinylated proteins were analyzed by gene ontology and divided into several expected categories, including autophagy, vesicular transport, transmembrane transport, and stress response (Fig 3-2C). A wide variety of the autophagy-related and vesicular transport proteins identified agreed well with what we expected based on ATG9A/autophagy literature. These included members of the ERGIC complexes (19), TRAPP complex (13, 20), AP-2 complex (21), RAB GAPs (22), VPS proteins (23), mitochondrial pore proteins (24), ULK1 complex proteins, and WIPI2 (10-12, 22, 24)—all sites of ATG9A localization or regulators of ATG9A trafficking pathways (Fig 3-2D). Based on these data, we selected a small subset of candidate proteins for validation by western blot. In agreement with the peptide counts in our mass spectrometry data, these proteins were predominately biotinylated by the C-terminal ATG9A-BL construct (Fig 3-2E).

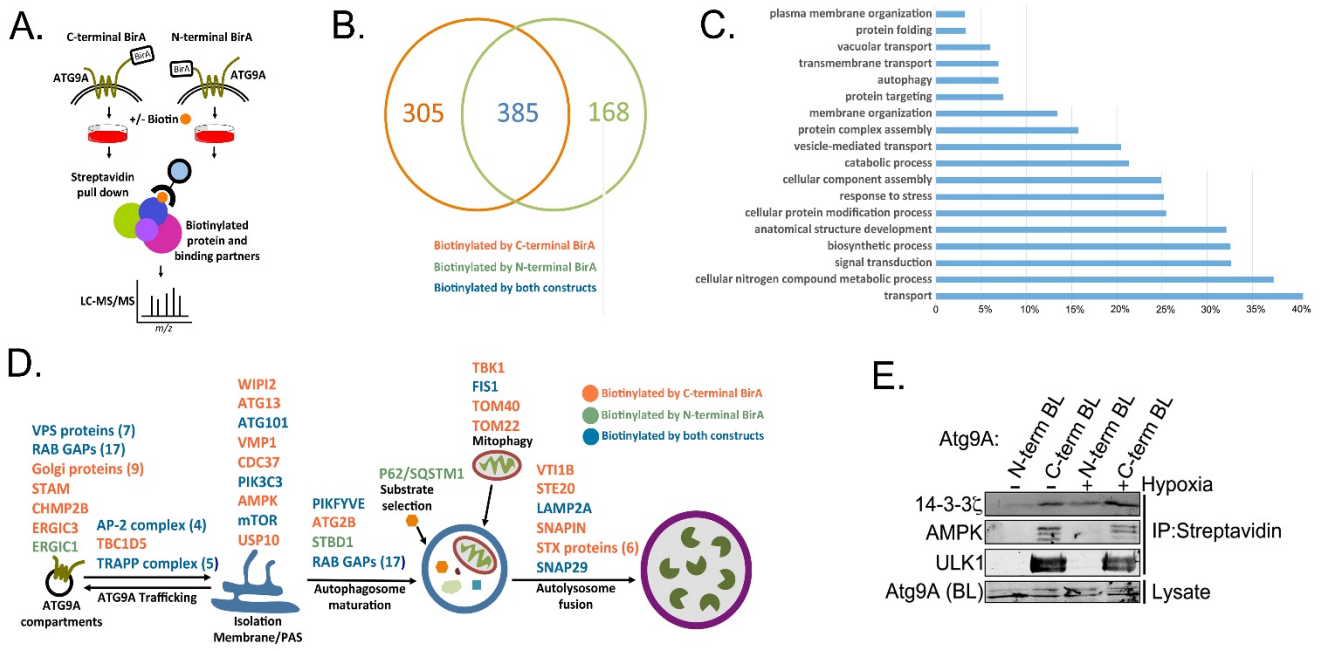

Figure 3-2 **A BioID approach identifies the ATG9A interactome.** (A) Workflow for the BioID coupled LC-MS/MS to identify termini specific interactome of ATG9A. (B) A Venn diagram illustrating the ATG9A interactome distributed with N versus C termini. (C) Gene ontology (GO) classification of BioID proteomics data. (D) Distribution of Bio-ID proteomics data GO categorized in to Autophagy pathways along the autophagasome synthesis process. (E) Validation of N versus C termini BioID proteomics hits using immunoblotting.

3.3.3 ATG9A co-fractionates with ULK1 complex proteins in size exclusion chromatography.

Our previously published data showed that ATG9A phosphorylation was dependent on ULK1 and AMPK (14), yet the motif surrounding S761 was a clear AMPK consensus site and bore little resemblance to known ULK1 sites (14). Given that AMPK exists within the ULK1 complex, we questioned whether ULK1 may simply bridge the kinase-substrate interaction between AMPK and ATG9A. Although, ATG9A and ULK1 are known to co-localize at the PAS/IM (10, 11, 25), to our knowledge no physical interaction had been shown. For these reasons, we were intrigued by the identification of ULK1 complex proteins (AMPK, ATG101, ATG13) biotinylated by C-terminal ATG9A-BL. As a first step toward probing potential ATG9A-ULK1 complex interactions, we wanted to determine whether ATG9A associates with large molecular weight

fractions consistent with canonical ULK1 complex proteins. We subjected HEK-293 and HCT-116 lysates to gel filtration on a Suprose 6 10/300 GL column, which separates protein complexes from ~6000 (the approximate size of the ULK1 complex) to ~200 kDa (ATG9A oligomer range). Interestingly, ATG9A fractionated in high molecular weight complexes in line with all of the ULK1 complex proteins tested (ULK1, FIP200, ATG13, AMPK, RAPTOR) (Fig 3-3A).

To gain a clearer picture of which fractions represent active, intact ULK1 complex, we probed for phosphorylated Ser555 (pS555) of ULK1, which is a substrate of AMPK within the ULK1 complex. Although we also detected total ULK1 in low molecular weight fractions, pS555, a ULK1 residue phosphorylated by AMPK within the ULK1 complex, was predominately restricted to three high molecular weight fractions shared with ATG9A. Consistent with these data, active AMPK, marked by phospho-T172 (an activating phosphorylation on the α subunit of AMPK), was also present in the same ATG9A-containing high molecular weight fractions. Notably, other areas of active AMPK and total RAPTOR were present across the size fractions, which is likely explained by other pools of mTORC1 and AMPK that are not linked to the ULK1 complex (26, 27) (Fig 3-3A).

To determine whether phosphorylated ATG9A is also present within the high molecular fractions, we developed an antibody that recognizes endogenous S761 phosphorylation. As shown in figure 3-3A, second panel down, pS761 is almost exclusively confined to the three high molecular weight fractions that correspond to the highest signals of pS555 and pT172. Figure 3-3B shows quantitation of the intensity of pS761, pS555 and PT172 signal across all 19 fractions (X axis numbering corresponds to lanes 1-19 on gel) and illustrates the overlap between the phospho signals. We also examined whether the spread of ATG9A and ULK1 complex proteins changed significantly in hypoxia-treated cells. Although hypoxia did not alter the general distribution of

ULK1 complex proteins in low versus high molecular weight fractions (Fig 3-3C), we did observe a clear shift in phosphorylated ATG9A between the two treatments. While in normoxia, pS761 is only detected in the ULK1 complex fractions, hypoxia triggers a shift of pS761 into the 200-500 kDa size range that likely contains the lower molecular weight ATG9A vesicles. This shift in pS761 relative to pS555 and pT172 is quantified in figure 3-3D.

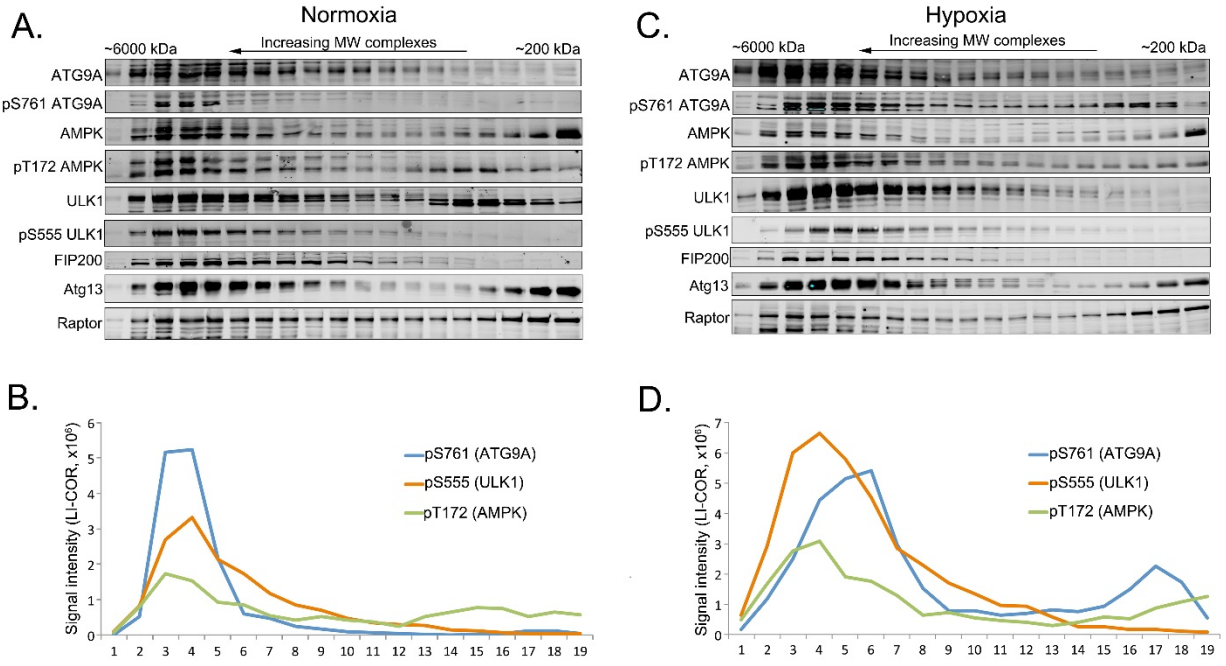

Figure 3-3 **ATG9A co-fractionates with ULK1 complex proteins in size exclusion chromatography.** (A) HEK293T cells were treated with normoxia for 12 hours. Cells were lysed and cleared supernatant were subjected to gel filtration. Resulting fractions were immunoblotted for indicated proteins (B) Signal intensities of mentioned proteins were graphed across the fraction number for (A). (B) HEK293T cells were treated with hypoxia for 12 hours. Cells were lysed and cleared supernatant were subjected to gel filtration. Resulting fractions were immunoblotted for indicated proteins (D) Signal intensities of mentioned proteins were graphed across the fraction number for (B).

3.3.4 ATG9A co-immunoprecipitates with ULK1 complex components at high molecular weight fractions.

To determine whether the gel filtration correlations between ATG9A and ULK1 complex proteins represented physical interactions, we first performed simple co-IP experiments in HEK-293 cells

using HA-tagged ATG9A as bait. We observed ULK1 and ATG13 co-immunoprecipitating with ATG9A (Fig 3-4A). To probe further, we subjected HA-ATG9A-expressing cells to gel filtration and pooled fractions into high (marked by pS555), mid and low molecular weight pools, followed by IP of HA-ATG9A from each pool (Fig 3-4B). Consistent with the initial gel filtration results, ULK1 and ATG13 co-immunoprecipitated with HA-ATG9A from high and mid molecular weight fractions (Fig 3-4C). Conversely, HA-ULK1 also co-immunoprecipitated with ATG9A and its expected ULK1 complex members in high and mid molecular weight pools.

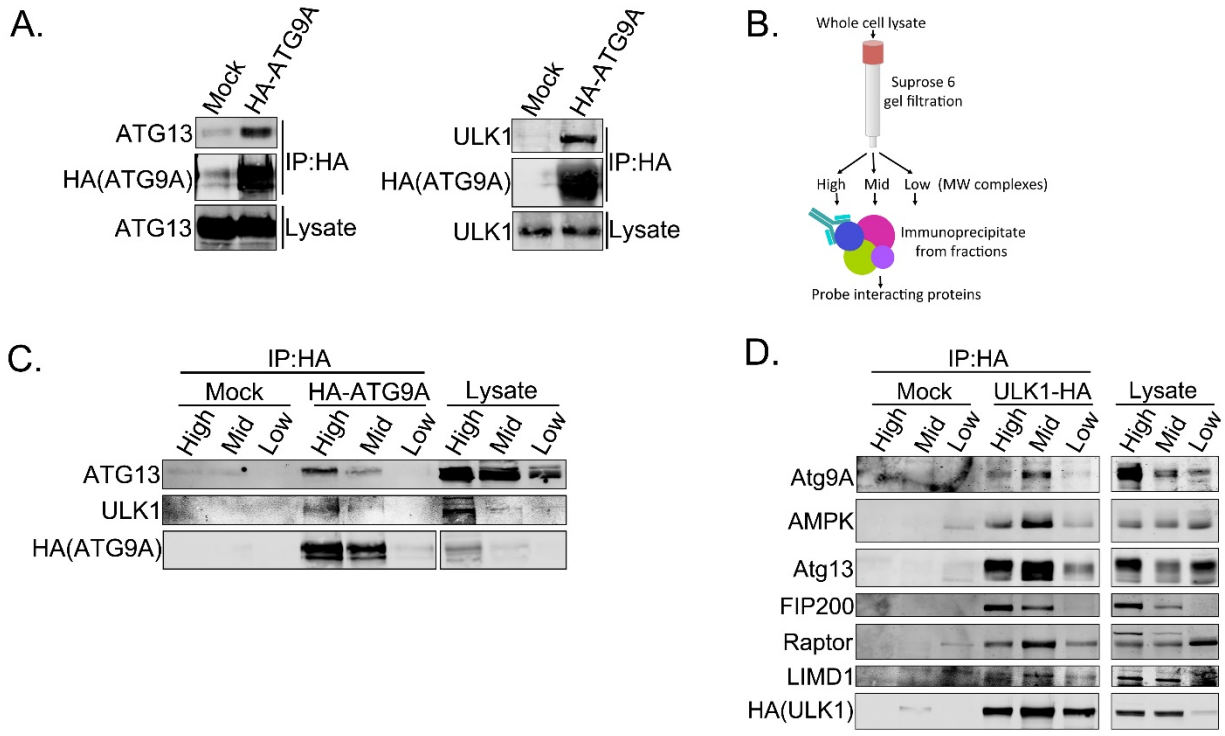

Figure 3-4 **ATG9A co-immunoprecipitates with ULK1 complex components at high molecular weight fractions.** (A) ULK1 complex proteins ATG13 (left panel) and ULK1 (right panel) immunoprecipitates with HA-ATG9A. (B) A workflow diagram illustrating co-immunoprecipitation of tagged ATG9A or ULK1 from pooled sixe exclusion chromatography fractions. (C) HCT116 cells were transfected with HA-ATG9A. After 48 hours cells were lysed and cleared cell lysates were subjected to size exclusion chromatography. High (fractions 1-6), mid (fractions 7-12) and low (fractions 13-19) molecular weight fractions were pooled together and co-immunoprecipitation was done using anti-HA resin. Immunoprecipitated proteins were separated on a SDS-PAGE and immunoblotted for indicated proteins. (D) HCT116 cells were transfected with HA-ULK1 and same procedure as above (C) was followed.

3.3.5 SDS lysis coupled BioID identifies direct versus indirect interactors of ATG9A.

We had initially set up our streptavidin pull-downs in figure 3-1 in the absence of SDS with the goal of maximizing capture of protein complexes. However, one advantage of BioID is that the streptavidin pull down can be done in lysis buffer with complex-disrupting concentrations of SDS (17, 18). This eliminates 'tag-along' interactions and selects for only those proteins that are directly biotinylated by ATG9A-BL (Fig 3-5A graphic), which gives an idea of the architecture of complex interactions. As shown in figure 3-5A, the addition of SDS disrupted the pull-down of ULK1 but had no effect on ATG13 pull-down, suggesting that ATG9A interacts with the ULK1 complex via ATG13. In addition, SDS disrupted the pull-down of ATG2, but increased the pull-down down of WIPI2, a mammalian homologue of yeast ATG18 that interacts with ATG9 (28). This increase in WIPI2 pull-down was initially puzzling, but may make sense given that WIPI2 associates with membrane, which is likely disrupted by SDS, making it more accessible to the streptavidin resin (Fig 3-5A).

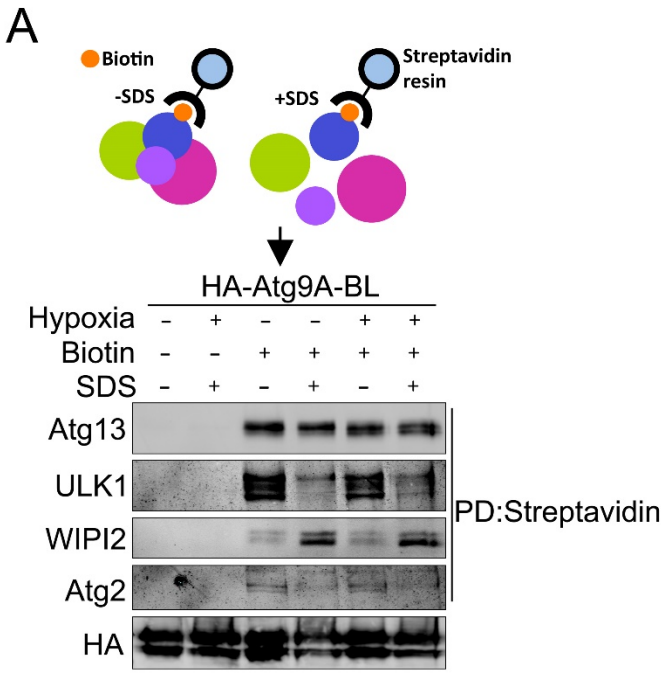

Figure 3-5 **SDS lysis coupled BioID identifies direct versus indirect interactors of ATG9A.** HCT116 cells were transfected with ATG9A-BL-HA construct. After 36 hours cells were treated with hypoxia or normoxia for 12 hours. After lysing in the presence or absence of 0.4% SDS, immunoprecipitation was done using streptavidin resin and immunoblotted for the indicated proteins.

3.3.6 Phosphorylation at S761 is necessary for the retrieval of ATG9A from ULK1 complex.

Our previously published results showed that ULK1 was required for AMPK-mediated phosphorylation of ATG9A (14), which led us to posit that the ULK1 complex may be scaffolding the kinase-substrate interaction between ATG9A and AMPK. As ATG13 is a core component of the ULK1 complex, our current data suggest that ATG13 may directly mediate the interaction between ATG9A and the ULK1 complex. If true, one prediction is that ATG13 would be required for ATG9A phosphorylation. To test this, we depleted cells of ATG13 and immunoblotted for endogenous S761 phosphorylation on ATG9A. As shown in figure 2-6A, siRNA depletion of ATG13 resulted in a significant loss of endogenous S761 phosphorylation.

If ATG9A is phosphorylated via interactions with the ULK1 complex, what effect does phosphorylation have on ATG9A function downstream of the IM/PAS? ATG9A is known to retrograde traffic from the IM/PAS back to endosomal, golgi and ATG9A reservoir sites where it is thought to pick up additional membrane to carry back the growing autophagosome (22, 29). Thus, ATG9A phosphorylation at the IM/PAS could be a trigger for retrograde trafficking. If so, we would predict that the S761A phospho-mutant of ATG9A should be sequestered with the ULK1 complex. In support of this idea, ATG9A-ATG13 co-IP experiments showed that the S761A pulls down nearly double the ATG13 compared with WT ATG9A (Fig 3-6B, first panel). Interestingly, this effect was strong under normoxic conditions and although the trend persisted in hypoxia, the difference was not significant. We reasoned that this may be due to increased autophagosomal biogenesis and flux in hypoxia, essentially giving ATG9A less time to accumulate at the PAS/IM before getting turned over or recycled through autophagy. To test this idea, we used wortmannin, an inhibitor the class III PI3K-Beclin complex, to stall autophagosome biogenesis, which we posited would allow for increased accumulation of the ATG9A S761A-ATG13 complex. Indeed, wortmannin treatment nearly doubled the interaction of ATG9A S761A with ATG13 in hypoxia (Fig 3-6B, second panel). We also tested the ability of the WT and S761A ATG9A-BL constructs to biotinylate ATG13. Similar to the co-IP results in panel B, the S761A mutant showed increased biotinylation of ATG13 and the effect was markedly increased by wortmannin treatment in hypoxia (Fig 3-6C).

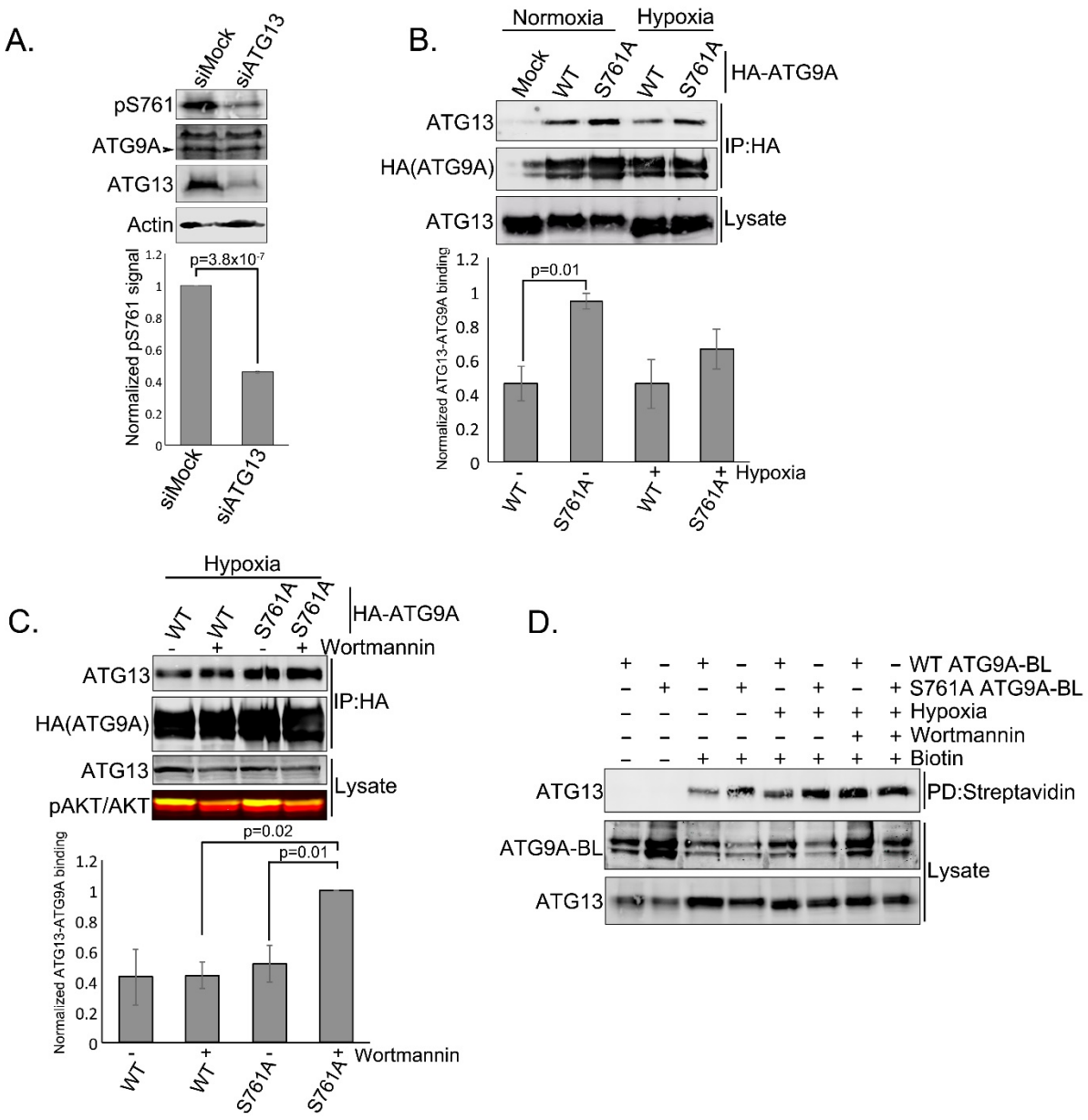

Figure 3-6. **Phosphorylation at S761 is necessary for the retrieval of ATG9A from ULK1 complex.** (A) HCT 116 cells were transfected with non-targeted siRNA or ATG13 siRNA. After 48 hours cell were lysed and immunoblotted for endogenous pS761 (n=4). (B) HCT116 cells were transfected with HA-WT-ATG9A or HA-S761A-ATG9A. After 36 hours cell were treated with normoxia or hypoxia for 12 hours and co-immunoprecipitated HA-ATG9A (WT or S761A) and immunoblotted for ATG13 (n=4). (C) HCT116 cells were transfected with HA-WT-ATG9A or HA-S761A-ATG9A. After 36 hours cells were treated with hypoxia in the presence of DMSO or 100nM wortmannin for 12 hours. Cells were lysed, HA-ATG9A (WT or S761A) was co-immunoprecipitated and immunoblotted for ATG13. (D) HCT 116 cells were transfected with WT-ATG9A-BL or S761A-ATG9A-BL. After 36 hours cells were treated with normoxia and hypoxia in the presence of 50μM Biotin and 100nM wortmannin or DMSO as indicated for 12 hours. Cells were lysed and biotinylated proteins were immunoprecipitated using streptavidin resin and immunoblotted for ATG13.

3.4 DISCUSSION

In this study, we used a biotin-ligase-based approach to characterize the network of proximity-based ATG9A-interacting proteins. By fusing the BirA biotin ligase domain to both ends of ATG9A, we could discriminate between proteins that are proximal to the N- or C-terminus of ATG9A. With this approach, we identified over 800 proteins, most of which interact with the C-terminus of ATG9A. Only 168 of the proteins showed preferential interaction with the N-terminus. Given that the C terminus is nearly 400 amino acids long and predicted to be unstructured, while the N terminus is approximately 50 amino acids, it is possible that the long C terminus extends the radius by which BirA can biotinylate neighboring proteins. Nevertheless, the large number of C-terminal ATG9A interactions (and the long unstructured C terminus itself) agrees with our preliminary model, in which the C terminus is a docking site for multiple protein interactions (Fig 3-1).

Standard approaches to probe protein interactomes have relied on direct co-IP, which typically selects for direct interactions while excluding neighboring proteins that are likely functionally important. These types of approaches are also difficult with transmembrane proteins, as the membrane component may preclude efficient co-IP and the 2-dimensional nature of the membrane interface reduces the binding affinities required to maintain stable interactions (18). Proximity labeling approaches have the advantage of widening the view of a protein's interactome and essentially creating a log of proteins that have been in close proximity to a transmembrane protein without the need for direct co-IP.

One critique of the BirA approach is the potential of promiscuous biotinylation and the resulting pull down of proteins that may not be biologically relevant. However, this problem is at least partially mitigated with transmembrane proteins that are fixed in position and interact in a 2-

dimensional plane. One of the most reassuring aspects of the ATG9A-BL proteomics results (Fig 3-2) is abundance of proteins present in known ATG9A compartments, such as the golgi, ER, and endosomes. A large number of well-described autophagy regulating proteins were found that span the autophagy pathway from autophagosome biogenesis to autophagosome-lysosome fusion. These include members of the TRAPP complex, ERGIC complexes, RAB GAPs, VPS proteins, and AP-2 complex. Also, based on our interest understanding the role of ULK1 in ATG9A phosphorylation, one of the most striking features was the presence of ULK1 complex proteins.

In exploring the significance of ULK1 complex-ATG9A interactions further, we found that ATG9A exists in a high molecular weight (~6000 kDa) complex with ULK1, ATG13 and other members of the ULK1 complex. Interestingly, using an antibody that recognizes endogenous phosphorylation of ATG9A at S761, we found that ATG9A phosphorylation occurs within the high molecular weight complex in basal ("normoxic") conditions, but begins to appear in the lower molecular weight fractions in hypoxia. We interpret this to be movement of phospho-ATG9A from the high molecular weight complexes into lower molecular weight fractions consistent with the weight of ATG9A dimers or oligomers (200-400 kDa), which could reflect the trafficking of phosphorylated ATG9A vesicles away from the ULK1 complex at the IM/PAS. In addition, our observation that ATG13 is required for ATG9A phosphorylation and that the phospho-mutant of ATG9A appears to accumulate with ATG13 further suggests that ATG9A phosphorylation occurs at the ULK1 complex and is important for retrograde trafficking away from the PAS. This is also consistent with our observation that the ATG9A phosphomutant shows a perinuclear staining (consistent with IM/PAS localization) whereas WT ATG9A is more diffuse across the cytosol. All together, these data suggest a model wherein ATG9A traffics to the IM/PAS where it interacts with the ULK1 complex via ATG13, which bridges the kinase-substrate interaction between

ATG9A and AMPK. In turn, phosphorylation of ATG9A triggers its recycling back to ATG9A membrane reservoirs.

3.5 Materials and method

3.5.1 Cell culture and transfection.

HEK-293 cells and U2OS cells were cultured in Dulbecco's modified Eagle's medium (DMEM) supplemented with 10% fetal bovine serum (FBS) at 37°C in a 5% CO_2 incubator. HCT116 cells were cultured in McCoy's 5A medium supplemented with 10% FBS at 37°C in a 5% CO2 incubator. Mouse Embryonic Fibroblasts (MEFs) were cultured in Dulbecco's modified Eagle's medium (DMEM) supplemented with 10% fetal bovine serum (FBS) at 37°C in a 5% CO2 incubator. For all hypoxia treatments, cells were treated in glucose-free DMEM supplemented with 2 mM glucose and 10% dialyzed FBS (Invitrogen) at 37°C in a 1% O_2 incubator. HEK- 293 cells, U2OS cells, and HCT116 cells were transiently transfected with hemagglutinin (HA)-Atg9A (WT or S761A), HA-ULK1 (WT, S758A or kinase dead), and/or AMPK alpha2 K45R (Addgene plasmid number 15992) plasmids by using FuGENE6 (Promega), TurboFect (Thermo Scientific), or polyethylenimine (PEI) (Polyscience, Inc.) according to the manufacturer's protocols.

3.5.2 Antibodies and chemicals.

The following antibodies were used. Anti-HA (F-7), anti-FLAG (D-8), anti-14-3-3ζ (C-16), anti-actin R (I-19), and anti-kinesin (H-50) were purchased from Santa Cruz Biotechnology. Antibodies for ATG101(catalog number 13492), p-AKT (catalog number 9275), ATG2A(catalog number 15011), WIPI2 (catalog number 8567), TBK1 (catalog number 3013), FIP200 (catalog number 12436), ATG13 (catalog number 13273), LC3B (catalog number 3868), phospho-S761-ATG9A(custom made), p-Raptor (catalog number 2083), phospho-Thr 172-AMPK (catalog number 2535), phospho-S555-ULK1 (catalog number 5869), phospho-acetyl coenzyme A (acetyl-

CoA) carboxylase (catalog number 3661), phospho-Thr172 of AMPK a1 (catalog number 2535), LC3B (catalog number 2775S), ULK1 (catalog number 8054S), the phosphoserine 14-3-3ζ motif ("pMotif") (9601S), Atg9A (catalog number 9730S), AMPKα (catalog number 5831), and AS160 (catalog number 2447S) were purchased from Cell Signaling. Antibodies for AMPK α1 and AMPK α2 were custom made by Affinity BioReagents. Anti-ULK2 (catalog number ab56736) was purchased from Abcam.

The following inhibitors were used. Complete protease inhibitors were purchased from Roche and used according to the manufacturer's procedures. SB203580 (catalog number 13067), Dynasore (catalog number 14062), wortmannin (catalog number 10010591), and bafilomycin A1 (catalog number 11038) were purchased from Cayman Chemicals. Compound C (catalog number 171260) and UCN-01 (catalog number 539644) were purchased from Calbiochem. Site-directed mutagenesis kits (catalog number 200521-5) were purchased from Agilent Technologies.

3.5.3 Plasmids.

Atg9A-HA and Atg9A-RFP plasmids were kindly provided by Sharon Tooze, London Research Institute, United Kingdom. The dominant negative pAMPK alpha2 K45R construct was obtained from Addgene (catalog number 15992). Biotin ligase – MYC – ATG9A and ATG9A – HA – Biotin ligase were kindly provided by J.J.Lee, Brigham Young University. HA-hATG13 plasmid was purchased from Addgene (catalog number 31967).

3.5.4 RNA interference.

ULK1 small interfering RNA (siRNA) (catalog number M-005049-00) and PRKAA1 siRNA (catalog number M-005027-02) were purchased from Thermo Scientific (Dharmacon siGENOME

SMARTpool). ULK2 siRNA (catalog number 956) and PRKAA2 siRNA (catalog number 103599) were purchased from Ambion by Life Technologies, Inc. ATG13 siRNA SMARTpool purchased by Dharmacon. siRNA was transfected by using Lipofectamine RNAiMAX (Life Technologies) at a 66 nM or 100 nM final concentration, according to the manufacturer's instructions.

3.5.5 Immunoprecipitation and immunoblotting.

To prepare whole-cell extracts, cells were washed twice and harvested with ice-cold phosphate – buffered saline (PBS). Cell pellets were resuspended in either coimmunoprecipitation (co-IP) buffer (10 mM HEPES [pH 7.5], 150 mM KCl, 0.1% NP-40) or Atg9A lysis buffer (20 mM Tris-HCl [pH 7.5], 150 mM NaCl, 0.3% [wt/vol] Triton X-100, and 5 mM EDTA) supplemented with pro- tease and phosphatase inhibitors and incubated for 15 min on ice or at 4°C with gentle rotation. Lysates were syringed through a 25-gauge needle 10 times and centrifuged at 21,000 rpm for 10 min at 4°C. For coimmunoprecipitation, cells were transfected with HA-Atg9A for 48 hours and lysates were incubated with anti-HA–agarose beads for1h at 4°C with gentle rotation. The beads were then washed once with lysis buffer and three times with cold PBS. The coimmunoprecipitated proteins were eluted with modified Laemmli sample buffer by boiling at 100°C for 5 min. The proteins were analyzed, followed by immunoblotting using infrared fluorescent secondary antibodies and a Li-Cor Odyssey imaging system.

For proximity dependent biotin ligase assay based co-immunoprecipitation; cells were transfected with biotin ligase constructs for 48 hours, treated with 5μM Biotin for 12 hours and lysed in ATG9A lysis buffer. Lysates were syringed through a 25-gauge needle 10 times and centrifuged at 21,000 rpm for 10 min at 4°C. Cleared lysates were incubated with streptavidin resin for 1 hour

at 4°C with gentle rotation. The resin was then washed twice with lysis buffer and three times with cold PBS. The coimmunoprecipitated proteins were eluted with modified Laemmli sample buffer by boiling at 100°C for 5 min. The proteins were analyzed, followed by immunoblotting using infrared fluorescent secondary antibodies and a Li-Cor Odyssey imaging system.

For proximity dependent biotin ligase assay based immunoprecipitation of biotinylated proteins; cells were transfected with biotin ligase constructs for 48 hours, treated with 5μM Biotin for 12 hours and lysed in SDS lysis buffer (50mM Tris-pH7.4, 500mM NaCl, 0.4% SDS, 5mM EDTA, 1mM DTT). Then Triton-X100 was added to final concentration of 2%. This was followed by addition of equal volume of ice-cold 50mM Tris (pH 7.4). Lysates were syringed through a 25-gauge needle 10 times and centrifuged at 21,000 rpm for 10 min at 4°C. Cleared lysates were incubated with streptavidin resin for 1 hour at 4°C with gentle rotation. The resin was then washed twice with lysis buffer and three times with cold PBS. The coimmunoprecipitated proteins were eluted with modified Laemmli sample buffer by boiling at 100°C for 5 min. The proteins were analyzed, followed by immunoblotting using infrared fluorescent secondary antibodies and a Li-Cor Odyssey imaging system.

3.5.6 Inhibitor assays.

The following inhibitors and concentrations were used in cell assays: LY294002 at 50 μM; UCN01 at 1 μM, 500 nM, and 300 nM; compound C at 20 μM; SB203580 at 2 μM; and U0126 at 20 μM.

Immunostaining and confocal microscopy.

Cells were seeded into 6-well plates on collagenized glass coverslips and allowed to grow overnight. Following transfection of Atg9A-RFP and GFP-ATG13, cells were washed three times with PBS. Cells were then fixed in 4% paraformaldehyde in PBS for 15 min with light agitation at

room temperature. Following fixing cells were washed three times with PBS and then permeabilized and blocked for 30 min with 1% whole goat serum in 0.1% Tween in PBS (0.1% PBS-T). Following permeabilization and blocking, 4-6-diamidino-2-phenylindole (DAPI) (Molecular Probes) was added for 30 min in 0.1% PBS-T with light agitation at room temperature. Following secondary antibody incubation, cells were washed three times for 10 min with PBS and mounted onto slides with Pro- Long Gold Antifade reagent (Molecular Probes). Micrographs were taken with an Olympus FluoView FV1000 confocal laser scanning microscope mounted on an Olympus IX81 inverted microscope with an oil-immersed 60X objective. Sequential scans were taken with consistent settings for DAPI, GFP, and RFP.

3.5.7 Gel filtration assay.

Cells were lysed in ATG9A lysis buffer. Lysates were centrifuged three times at 4°C for 15 min at 13,200 rpm, and the protein concentration of the supernatant was determined by using the Bio-Rad protein assay reagent. Five hundred microliters of 8 mg/ml of lysates was loaded onto a Superose6 10/300GL column at a flow rate of 0.25 ml/min to collect fractions.

Co-immunoprecipitation coupled Mass spectrometry to identify interacting partners.

HA- tagged ATG9A (or mock control) co-immunoprecipitates were digested in solution after normalization to equivalent total protein concentrations by using a mini-Bradford assay (Bio-Rad, Inc.). Briefly, samples were supplemented with 0.25% Rapigest SF (Waters Corp.) in 50 mM ammonium bicarbonate (AmBic) and then reduced at 80°C with 20 mM dithiothreitol, followed by alkylation at room temperature with 40 mM iodoacetamide. Finally, digestion with trypsin (sequencing grade, modified; Pro- mega) was performed overnight at 37°C (50:1 substrate/enzyme ratio). Digestion was quenched and Rapigest was degraded by using acidification to 1% (vol/vol)

trifluoroacetic acid (TFA) for2h at 60°C. Finally, samples were dried and resuspended at 1 mg/ml in 200 mM ammonium formate (pH 10) for analysis by two-dimensional liquid chromatography-tandem mass spectrometry (LC/LC-MS/MS).

3.5.8 Bio-ID coupled Mass spectrometry to identify interacting partners.

Co-immunoprecipitated proteins by Streptavidin (with biotin or no biotin control) resin were eluted with modified Laemmli sample buffer by boiling at 100°C for 5 min. Eluted samples were measured for total protein, run in a gel, digested after normalization to equivalent total protein concentrations. Briefly, samples were supplemented with 0.25% Rapigest SF (Waters Corp.) in 50 mM ammonium bicarbonate (AmBic) and then reduced at 80°C with 20 mM dithiothreitol, followed by alkylation at room temperature with 40 mM iodoacetamide. Finally, digestion with trypsin (sequencing grade, modified; Pro- mega) was performed overnight at 37°C (50:1 substrate/enzyme ratio). Digestion was quenched and Rapigest was degraded by using acidification to 1% (vol/vol) trifluoroacetic acid (TFA) for2h at 60°C. Finally, samples were dried and resuspended at 1 mg/ml in 200 mM ammoniumformate (pH 10) for analysis by two-dimensional liquid chromatography-tandem mass spectrometry (LC/LC-MS/MS)

LC-MS data processing and quantitation.

The data were searched against the UNIPROT database with Homo sapiens taxonomy and reviewed status (http://www.uniprot.org/). The database was appended with several common contaminant or internal standard proteins (ALBU_BOVIN, ADH1_YEAST, ENO1_YEAST, PYGM_RABIT, and CASA1_BOVIN) and a 1X reverse database for peptide false-discovery-rate determination. MS/MS spectra generated by DDA were compiled into .mgf format by using Mascot Distiller v2.2 and submitted to the Mascot v2.2 (Matrix Sciences, Inc.) search engine. For

HDMSE and MSE data, Protein- Lynx Global Server 2.5 (Waters Corp.) was used to generate searchable files, which were then submitted to the IdentityE search engine (Waters Corp., Milford, MA). The automated merge function within PLGS 2.5 was used to combine spectral information from each of the five fractions prior to searches with IdentityE. The precursor ion mass tolerances were 10 ppm and 5 ppm for Mascot and PLGS searches, respectively, and the product ion tolerances were 0.04 Da for Mascot and 13 ppm for PLGS. For both search engines, the enzyme specificity was set to tryptic, and a maximum of 2 missed cleavages were allowed. Carbamidomethyl cysteine was included as a fixed modification, and variable modifications included oxidized methionine, deamidated asparagine and glutamine, acetylated lysine, and phosphorylated serine and threonine. PLGS searches were per- formed by requiring at least 3 products per precursor, 7 product ions per protein, and 1 peptide per protein. Qualitative data were curated in Scaffold v4 (Proteome Software, Inc.). Relative quantitation between hypoxia and normoxia conditions was performed based on first analyzer (MS1) extracted-ion chromatograms by using the Skyline v2.5.1 software environment (23). The raw data associated with this analysis are available on the Panorama server (http://goo.gl/aO68ge).

3.6 REFERENCES

1. **Hosokawa N, Hara T, Kaizuka T, Kishi C, Takamura A, Miura Y, Iemura S, Natsume T, Takehana K, Yamada N, Guan JL, Oshiro N, Mizushima N.** 2009. Nutrient-dependent mTORC1 association with the ULK1-Atg13-FIP200 complex required for autophagy. Mol Biol Cell **20:**1981-1991.
2. **Kim J, Kundu M, Viollet B, Guan KL.** 2011. AMPK and mTOR regulate autophagy through direct phosphorylation of Ulk1. Nat Cell Biol **13:**132-141.
3. **Gwinn DM, Shackelford DB, Egan DF, Mihaylova MM, Mery A, Vasquez DS, Turk BE, Shaw RJ.** 2008. AMPK phosphorylation of raptor mediates a metabolic checkpoint. Mol Cell **30:**214-226.
4. **Inoki K, Zhu T, Guan KL.** 2003. TSC2 mediates cellular energy response to control cell growth and survival. Cell **115:**577-590.

5. **Egan D, Kim J, Shaw RJ, Guan KL.** 2011. The autophagy initiating kinase ULK1 is regulated via opposing phosphorylation by AMPK and mTOR. Autophagy **7:**643-644.
6. **Lee JW, Park S, Takahashi Y, Wang HG.** 2010. The association of AMPK with ULK1 regulates autophagy. PLoS One **5:**e15394.
7. **Shang L, Chen S, Du F, Li S, Zhao L, Wang X.** 2011. Nutrient starvation elicits an acute autophagic response mediated by Ulk1 dephosphorylation and its subsequent dissociation from AMPK. Proc Natl Acad Sci U S A **108:**4788-4793.
8. **Saitoh T, Fujita N, Hayashi T, Takahara K, Satoh T, Lee H, Matsunaga K, Kageyama S, Omori H, Noda T, Yamamoto N, Kawai T, Ishii K, Takeuchi O, Yoshimori T, Akira S.** 2009. Atg9a controls dsDNA-driven dynamic translocation of STING and the innate immune response. Proc Natl Acad Sci U S A **106:**20842-20846.
9. **Kuma A, Hatano M, Matsui M, Yamamoto A, Nakaya H, Yoshimori T, Ohsumi Y, Tokuhisa T, Mizushima N.** 2004. The role of autophagy during the early neonatal starvation period. Nature **432:**1032-1036.
10. **Kishi-Itakura C, Koyama-Honda I, Itakura E, Mizushima N.** 2014. Ultrastructural analysis of autophagosome organization using mammalian autophagy-deficient cells. J Cell Sci **127:**4089-4102.
11. **Young AR, Chan EY, Hu XW, Kochl R, Crawshaw SG, High S, Hailey DW, Lippincott-Schwartz J, Tooze SA.** 2006. Starvation and ULK1-dependent cycling of mammalian Atg9 between the TGN and endosomes. J Cell Sci **119:**3888-3900.
12. **Orsi A, Razi M, Dooley HC, Robinson D, Weston AE, Collinson LM, Tooze SA.** 2012. Dynamic and transient interactions of Atg9 with autophagosomes, but not membrane integration, are required for autophagy. Mol Biol Cell **23:**1860-1873.
13. **Lamb CA, Nuhlen S, Judith D, Frith D, Snijders AP, Behrends C, Tooze SA.** 2016. TBC1D14 regulates autophagy via the TRAPP complex and ATG9 traffic. EMBO J **35:**281-301.
14. **Weerasekara VK, Panek DJ, Broadbent DG, Mortenson JB, Mathis AD, Logan GN, Prince JT, Thomson DM, Thompson JW, Andersen JL.** 2014. Metabolic stress-induced rearrangement of the 14-3-3zeta interactome promotes autophagy via a ULK1- and AMPK-regulated 14-3-3zeta interaction with phosphorylated Atg9A. Mol Cell Biol doi:10.1128/MCB.00740-14.
15. **Yaffe MB.** 2002. How do 14-3-3 proteins work?-- Gatekeeper phosphorylation and the molecular anvil hypothesis. FEBS Lett **513:**53-57.
16. **He C, Baba M, Cao Y, Klionsky DJ.** 2008. Self-interaction is critical for Atg9 transport and function at the phagophore assembly site during autophagy. Mol Biol Cell **19:**5506-5516.
17. **Roux KJ, Kim DI, Raida M, Burke B.** 2012. A promiscuous biotin ligase fusion protein identifies proximal and interacting proteins in mammalian cells. J Cell Biol **196:**801-810.
18. **Rees JS, Li XW, Perrett S, Lilley KS, Jackson AP.** 2015. Protein Neighbors and Proximity Proteomics. Mol Cell Proteomics **14:**2848-2856.
19. **Karanasios E, Walker SA, Okkenhaug H, Manifava M, Hummel E, Zimmermann H, Ahmed Q, Domart MC, Collinson L, Ktistakis NT.** 2016. Autophagy initiation by ULK complex assembly on ER tubulovesicular regions marked by ATG9 vesicles. Nat Commun **7:**12420.

20. **Shirahama-Noda K, Kira S, Yoshimori T, Noda T.** 2013. TRAPPIII is responsible for vesicular transport from early endosomes to Golgi, facilitating Atg9 cycling in autophagy. J Cell Sci **126:**4963-4973.
21. **Imai K, Hao F, Fujita N, Tsuji Y, Oe Y, Araki Y, Hamasaki M, Noda T, Yoshimori T.** 2016. Atg9A trafficking through the recycling endosomes is required for autophagosome formation. J Cell Sci **129:**3781-3791.
22. **Reggiori F, Tooze SA.** 2012. Autophagy regulation through Atg9 traffic. J Cell Biol **198:**151-153.
23. **Nickerson DP, Brett CL, Merz AJ.** 2009. Vps-C complexes: gatekeepers of endolysosomal traffic. Curr Opin Cell Biol **21:**543-551.
24. **Itakura E, Kishi-Itakura C, Koyama-Honda I, Mizushima N.** 2012. Structures containing Atg9A and the ULK1 complex independently target depolarized mitochondria at initial stages of Parkin-mediated mitophagy. J Cell Sci **125:**1488-1499.
25. **Karanasios E, Stapleton E, Manifava M, Kaizuka T, Mizushima N, Walker SA, Ktistakis NT.** 2013. Dynamic association of the ULK1 complex with omegasomes during autophagy induction. J Cell Sci **126:**5224-5238.
26. **Mihaylova MM, Shaw RJ.** 2011. The AMPK signalling pathway coordinates cell growth, autophagy and metabolism. Nat Cell Biol **13:**1016-1023.
27. **Bar-Peled L, Sabatini DM.** 2014. Regulation of mTORC1 by amino acids. Trends Cell Biol **24:**400-406.
28. **Reggiori F, Tucker KA, Stromhaug PE, Klionsky DJ.** 2004. The Atg1-Atg13 complex regulates Atg9 and Atg23 retrieval transport from the pre-autophagosomal structure. Dev Cell **6:**79-90.
29. **Lamb CA, Yoshimori T, Tooze SA.** 2013. The autophagosome: origins unknown, biogenesis complex. Nat Rev Mol Cell Biol **14:**759-774.

CHAPTER 4 Discussion

Our work on ATG9A began with an effort to use 14-3-3ζ as a tool to capture pro-survival protein phosphorylations that help cells survive hypoxic stress. Using this approach, we identified Atg9A as a hypoxia-triggered 14-3-3ζ interacting protein. We then identified the 14-3-3ζ binding site as phospho-S761 within the C-terminus of ATG9A and found that loss of this phosphorylation rendered ATG9A defective in its autophagy function. Indeed, cells expressing a non-phosphorylatable mutant of ATG9A showed reduced LC3-II levels as well as a significant drop in autophagosome numbers and size. Furthermore, the ATG9A S761A mutant failed to traffic properly in response to autophagic signals, indicating that phosphorylation of S761 and 14-3-3ζ binding were necessary for ATG9A activation. Importantly, this was the first demonstration of a regulatory phosphorylation on mammalian ATG9A[1].

Prior to this work, other laboratories, including Dr. Sharon Tooze's group, had identified a number of proteins as required for proper ATG9A trafficking. These included p38α-MAPK[2], ULK1, ATG16L1, WIPI proteins and AMPK[3–16]. However we did not know how these proteins and cellular energy levels impacted ATG9A activity on a mechanistic level. Indeed, there was no direct mechanism linking the energy-sensing ULK1 complex or any other energy sensing mechanism directly to ATG9A. In this context, our observation that ULK1 and AMPK were required for ATG9A S761 phosphorylation was intriguing in that it had the potential to explain such a link. We went on to show that AMPK was the direct kinase that mediated S761 phosphorylation, thus providing a direct link between the energy sensing activities of AMPK and the activation of ATG9A.

One critical question that remained from our initial work stemmed from the puzzling observation that ULK1 and AMPK were required for the low basal phosphorylation of ATG9A in nutrient replete conditions, but only AMPK was required for the hypoxia-induced phosphorylation of ATG9A[1]. In an effort to understand this differential requirement for AMPK and ULK1, we delved into the literature and noted that in nutrient replete conditions ULK1 forms a complex with FIP200, ATG13, ATG101, Raptor and AMPK. However, others had shown that under nutrient depleted conditions, AMPK dissociates from the ULK1 complex[5,17–19]. These data led us to ask whether ULK1 may simply act as a scaffold to bring ATG9A and AMPK together under nutrient replete conditions. This idea of a protein scaffolding AMPK to its substrate under nutrient replete conditions was intriguing given that it would likely be the only way to allow for an AMPK-mediated phosphorylation to occur under such conditions where AMPK is not fully active.

In support of the idea that ATG9A interacts with the ULK1, other groups had reported that ATG9A co-localizes with ULK1[16,20]. Accordingly with their observations, we found that ATG9A co-IPs with ULK1 together with AMPK in nutrient replete conditions. We also observed that the expression of a ULK1 mutant (S758A) that cannot bind to AMPK caused a decrease in the basal phosphorylation of ATG9A, suggesting that AMPK must be sequestered within the ULK1 complex for basal ATG9A phosphorylation to occur. Furthermore, these data suggested that ATG9A may be a component of ULK1 complex. To further evaluate this, we used size exclusion chromatography and proximity dependent biotin ligase coupled LC-MS/MS[21]. Our data showed ATG9A co-fractionates with all ULK1 complex proteins in the high molecular fractions previously shown to mark the ULK1 complex. Furthermore, using an antibody to detect endogenous S761 phosphorylation, we found that phosphorylation of ATG9A occurs within these high molecular weight ULK1 fractions under basal conditions, but migrates into lower molecular weight fractions

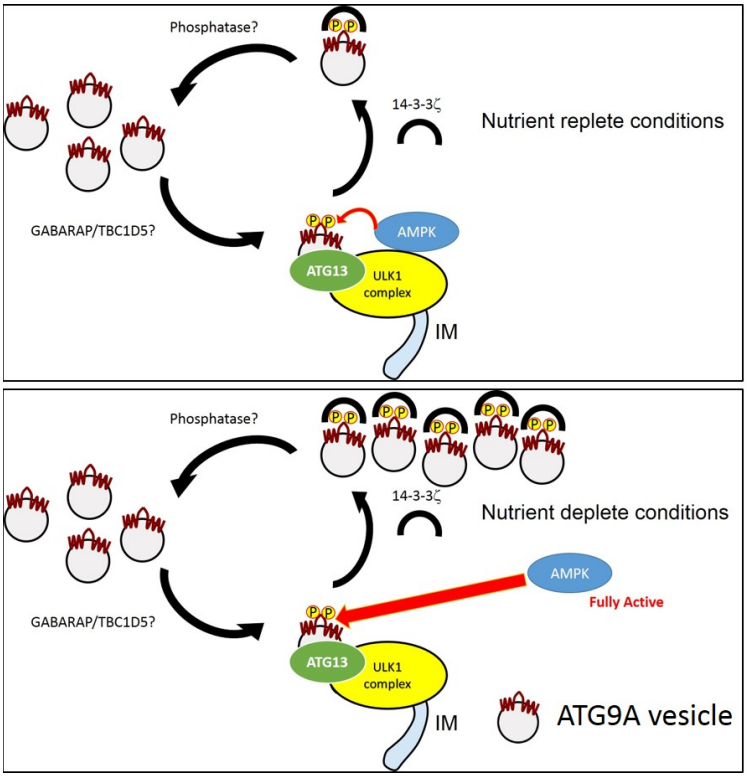

Figure 4-1 **Model: Differential Regulation of ATG9A phosphorylation in normoxia or hypoxia and its function in ATG9A trafficking.** In normoxia AMPK is less active and exists as a component of ULK1 complex. ATG9A is recruited onto PAS by ATG13. To maintain basal autophagy and ATG9A recycling, ATG9A is phosphorylated on PAS by AMPK in a ULK1 dependent manner. In hypoxia, AMPK becomes highly active and dissociates from ULK1 complex. To compensate for increased rate of autophagasomes production ATG9A is recycled promptly towards peripheral endosomal compartment through direct phosphorylation by AMPK.

in hypoxia. We interpret this low molecular weight migration of the phospho-form of ATG9A to represent the small ATG9A vesicles reported by other groups[8–10,12,22–24].

In a complementary approach to size exclusion chromatography, we showed that a BirA biotin ligase-ATG9A fusion protein biotinylates ULK1 complex proteins such as ATG13, ATG101, FIP200, AMPK and mTORC1, suggesting that ATG9A is in close proximity to the ULK1 complex. This approach proved to be powerful in that it allowed us to gain some insight into the topology of the ATG9A-ULK1 complex interactions. It showed that ATG9A only interacted directly with ATG13 of the ULK1 complex, suggesting ATG13 is the physical link that tethers ATG9A to the ULK1 complex, which is consistent with observations in yeast[25]. One prediction of this model is that ATG13 would be required for ATG9A phosphorylation. Indeed, we showed that knockdown of ATG13 dramatically reduced the endogenous phosphorylation of ATG9A at S761.

Together, these data have led us to propose the following working model (Fig 5-1). Under nutrient replete conditions, ATG9A is recruited to the ULK1 complex via an interaction with ATG13. We propose that the ATG9A-ULK1 complex interaction occurs at the phagophore assembly site (PAS), which is consistent with previous observations from the Tooze laboratory on ATG9A-ULK1 colocalization[20]. We propose that it is within this complex at the PAS, that AMPK phosphorylates ATG9A at S761. In turn, 14-3-3ζ interacts with ATG9A at the phospho-S761 site, which promotes ATG9A trafficking away from the ULK1 complex back to peripheral endosomal structures, where ATG9A is thought to pick up membrane to return to the PAS[2,15,16,26]. Thus, our data suggest that phosphorylation of S761 promotes the "retrograde" recycling of ATG9A away from the PAS. Under starved conditions where AMPK dissociates from ULK1 complex, we propose that the full activation of AMPK makes its tethering within the ULK1 complex unnecessary for ATG9A phosphorylation (Fig 4-1). Indeed, in order to keep up with the requirement for increased ATG9A cycling in starved conditions, fully active AMPK phosphorylates ATG9A at a higher rate, which in turn increases retrograde trafficking of ATG9A back to endosomal structures. A critical yet still unidentified component of this model is a phosphatase that we predict would remove the phosphorylation and allow for ATG9A anterograde trafficking to the PAS. This phosphatase is likely to be activated by low nutrients in order to promote ATG9A anterograde trafficking during starvation. The net result of the phosphorylation-driven increase in ATG9A trafficking is an increased supply of membrane to support the growth of autophagosomes. Thus, in summary, this model provides the first insight into the molecular mechanism that links nutrient signaling pathways directly to the core autophagy regulator ATG9A.

4.1 References

1. Weerasekara, V. K. *et al.* Metabolic-Stress-Induced Rearrangement of the 14-3-3ζ Interactome Promotes Autophagy via a ULK1- and AMPK-Regulated 14-3-3ζ Interaction with Phosphorylated Atg9. *Mol. Cell. Biol.* **34,** 4379–4388 (2014).
2. Webber, J. L. & Tooze, S. A. Coordinated regulation of autophagy by p38α MAPK through mAtg9 and p38IP. *EMBO J.* **29,** 27–40 (2010).
3. Chen, D. *et al.* CCCP-Induced LC3 lipidation depends on Atg9 whereas FIP200/Atg13 and Beclin 1/Atg14 are dispensable. *Biochem. Biophys. Res. Commun.* **432,** 226–230 (2013).
4. Chan, E. Y. W., Longatti, A., McKnight, N. C. & Tooze, S. A. Kinase-Inactivated ULK Proteins Inhibit Autophagy via Their Conserved C-Terminal Domains Using an Atg13-Independent Mechanism. *Mol. Cell. Biol.* **29,** 157–171 (2009).
5. Ganley, I. G. *et al.* ULK1·ATG13·FIP200 Complex Mediates mTOR Signaling and Is Essential for Autophagy. *J. Biol. Chem.* **284,** 12297–12305 (2009).
6. He, S. *et al.* PtdIns(3)P-bound UVRAG coordinates Golgi-ER retrograde and Atg9 transport by differential interactions with the ER tether and the beclin 1 complex. *Nat. Cell Biol.* **15,** 1206–1219 (2013).
7. Hosokawa, N. *et al.* Nutrient-dependent mTORC1 Association with the ULK1–Atg13–FIP200 Complex Required for Autophagy. *Mol. Biol. Cell* **20,** 1981–1991 (2009).
8. Imai, K. *et al.* Atg9A trafficking through the recycling endosomes is required for autophagosome formation. *J. Cell Sci.* **129,** 3781–3791 (2016).
9. Itakura, E. & Mizushima, N. Characterization of autophagosome formation site by a hierarchical analysis of mammalian Atg proteins. *Autophagy* **6,** 764–776 (2010).

10. Itakura, E., Kishi-Itakura, C., Koyama-Honda, I. & Mizushima, N. Structures containing Atg9A and the ULK1 complex independently target depolarized mitochondria at initial stages of Parkin-mediated mitophagy. *J Cell Sci* **125,** 1488–1499 (2012).
11. Jin, M. & Klionsky, D. J. Transcriptional regulation of ATG9 by the Pho23-Rpd3 complex modulates the frequency of autophagosome formation. *Autophagy* **10,** 1681–1682 (2014).
12. Lamb, C. A. *et al.* TBC1D14 regulates autophagy via the TRAPP complex and ATG9 traffic. *EMBO J.* **35,** 281–301 (2016).
13. Zhong, Y. *et al.* Distinct regulation of autophagic activity by Atg14L and Rubicon associated with Beclin 1–phosphatidylinositol-3-kinase complex. *Nat. Cell Biol.* **11,** 468–476 (2009).
14. Zhang, X. *et al.* Aberrant methylation of ATG2B, ATG4D, ATG9A and ATG9B CpG island promoter is associated with decreased mRNA expression in sporadic breast carcinoma. *Gene* **590,** 285–292 (2016).
15. Zavodszky, E., Vicinanza, M. & Rubinsztein, D. C. Biology and trafficking of ATG9 and ATG16L1, two proteins that regulate autophagosome formation. *FEBS Lett.* **587,** 1988–1996 (2013).
16. Young, A. R. J. *et al.* Starvation and ULK1-dependent cycling of mammalian Atg9 between the TGN and endosomes. *J. Cell Sci.* **119,** 3888–3900 (2006).
17. Egan, D., Kim, J., Shaw, R. J. & Guan, K.-L. The autophagy initiating kinase ULK1 is regulated via opposing phosphorylation by AMPK and mTOR. *Autophagy* **7,** 643–644 (2011).
18. Kim, J., Kundu, M., Viollet, B. & Guan, K.-L. AMPK and mTOR regulate autophagy through direct phosphorylation of Ulk1. *Nat. Cell Biol.* **13,** 132–141 (2011).

19. Kim, J., Kundu, M., Viollet, B. & Guan, K.-L. AMPK and mTOR regulate autophagy through direct phosphorylation of Ulk1. *Nat. Cell Biol.* **13,** 132–141 (2011).

20. Orsi, A. *et al.* Dynamic and transient interactions of Atg9 with autophagosomes, but not membrane integration, are required for autophagy. *Mol. Biol. Cell* **23,** 1860–1873 (2012).

21. Roux, K. J., Kim, D. I. & Burke, B. BioID: a screen for protein-protein interactions. *Curr. Protoc. Protein Sci.* **74,** Unit 19.23. (2013).

22. He, C. & Klionsky, D. J. Atg9 Trafficking in Autophagy-Related Pathways. *Autophagy* **3,** 271–274 (2007).

23. Koyama-Honda, I., Itakura, E., Fujiwara, T. K. & Mizushima, N. Temporal analysis of recruitment of mammalian ATG proteins to the autophagosome formation site. *Autophagy* **9,** 1491–1499 (2013).

24. Puri, C., Renna, M., Bento, C. F., Moreau, K. & Rubinsztein, D. C. ATG16L1 meets ATG9 in recycling endosomes. *Autophagy* **10,** 182–184 (2014).

25. Suzuki, S. W. *et al.* Atg13 HORMA domain recruits Atg9 vesicles during autophagosome formation. *Proc. Natl. Acad. Sci. U. S. A.* **112,** 3350–3355 (2015).

26. Moreau, K., Puri, C. & Rubinsztein, D. C. Methods to analyze SNARE-dependent vesicular fusion events that regulate autophagosome biogenesis. *Methods* **75,** 19–24 (2015).